AFIT/GEP/PH/78D-13

LEVEL II

AD A064756

DDC FILE COPY

SYNTHESIS OF THE PLASMA CHEMISTRY OCCURRING IN HIGH POWER CO_2 LASERS

THESIS

David E. Toodle
AFIT/GEP/PH/78D-13 2nd Lt USAF

Approved for public release; distribution unlimited

(14) AFIT/GEP/PH/78D-13

(6) SYNTHESIS OF THE PLASMA CHEMISTRY OCCURRING IN HIGH POWER CO_2 LASERS.

(9) Master's thesis,

THESIS

(16) 2301 (17) 52.

Presented to the Faculty of the School of Engineering

of the Air Force Institute of Technology

Air University

in Partial Fulfillment of the

Requirements for the Degree of

Master of Science

(13) 94 p.

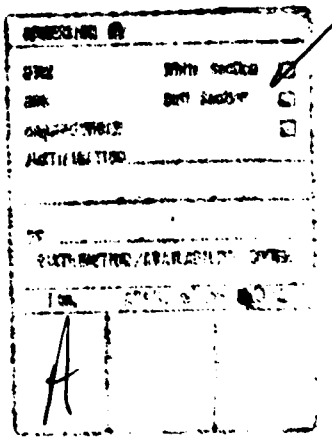

by

(10) David E. Toodle ~~B.S.~~

2nd Lt USAF

Graduate Engineering Physics

(11) December ~~1~~ 1978

Approved for public release; distribution unlimited

012 225

Preface

Carbon dioxide lasers have become the topic of increased research over the last few years. One area of active investigation is the plasma chemistry occurring in the laser discharge. These studies are ultimately related to the development of flowing and nonflowing sealed CO_2 lasers. Such laser systems offer versatility which is advantageous to the Air Force and industry. It is hoped that the present study aids in the understanding of plasma chemistry processes in the CO_2 laser discharge.

I would like to thank the whole staff of the Advanced Concepts Group of the Air Force Aero Propulsion Laboratory. Special thanks goes to my advisor, Alan Garscadden, for his guidance and Michael Stamm for the chemistry code used in the theoretical predictions. Thanks is also due to Richard Franklin for his helpful suggestions on the code and draft of this report. Last but not least, I would like to thank my wife, Hattie, for her patience and for preparing most of the figures used in this report.

David E. Toodle

Contents

List of Figures

Abstract

The neutral chemistry of the following mixtures have been studied by using a quadrupole mass spectrometer and a theoretical model: CO_2/Ar, N_2/Ar, CO_2/N_2/Ar, CO_2/He/Ar, and CO_2/N_2/He/Ar. CO_2 dissociation occurs by direct electron impact and appears to depend on initial CO_2 concentration and mixture. Very little N_2 dissociation occurs in a pure N_2 discharge; however, the dissociation of N_2 increases when it is added to a mixture containing CO_2. This dissociation is less than 1%. Consequently, the dominant nitrogen oxide in mixtures containing CO_2 and N_2 is NO, and the concentration of NO never exceeds 1%. The species CHO and CH_2O are present at high discharge currents if there is a small amount of water contamination in mixtures containing CO_2.

SYNTHESIS OF THE PLASMA CHEMISTRY OCCURRING IN HIGH POWER CO_2 LASERS

I. Introduction

Background

The most important problem facing closed-cycle CO_2 lasers is that under sealed-off conditions, the original $CO_2/N_2/He$ mixture changes considerably due to the plasma chemistry occurring in the laser discharge. Reactions of prime concern are the dissociation of CO_2 into CO and O, the formation of nitrogen oxides, and the formation of significant amounts of negative ion species. The irreversible loss of CO_2 reduces the output power, while the nitrogen oxides and negative ion impurities alter the properties of the laser discharge.

Two methods are used to solve the problem of CO_2 dissociation (Ref 12:2039). One method is to employ heated platinum or copper as a catalyst. The other method is to use the catalytic action of H_2O or H_2. Small amounts of water vapor or H_2 in the discharge reform the CO_2 through the following reactions:

$$CO + OH \rightarrow CO_2 + H \qquad (1.1)$$

$$CO + HO_2 \rightarrow CO_2 + OH \qquad (1.2)$$

The OH comes from the dissociation of H_2O, and the HO_2 comes from the dissociation of H_2 and subsequent combination of H with O_2.

The nitrogen oxides that are formed quench the CO_2 vibrational excitation and also compete with the CO_2 for vibrational excitation by electron inelastic collisions. These impurities also affect the laser gain and discharge impedance (Ref 4). The negative ion population can become comparable to (and in some cases even exceed) the electron population, resulting in discharge arcing (Ref 13:268). The effects of the nitrogen oxides and negative ion species mentioned here limit long-term operation of closed-cycle systems.

Previous experimental studies of the plasma chemistry have usually involved pure CO_2 (Refs 1, 7, and 8) or the total laser mixture consisting of $CO_2/N_2/He$ (Refs 2, 11, 12, 18, 22, and 24). CO_2 dissociation in a pure CO_2 discharge does not necessarily occur at the same rate as CO_2 dissociation in a mixture. Although it is a simple job to track the buildup of certain species in a $CO_2/N_2/He$ discharge, the identification of the primary reactions involved is a complicated task. In order to get a clear picture of the reactions involved, it is advantageous to start initially with simple mixtures. Then, known amounts of additional gases are titrated in. The above procedure represents the "synthesis" approach in studying the chemistry of the laser discharge. Important initial steps

toward this type of study have been made by Buser and Sullivan (Ref 5), and Smith and Austin (Ref 20).

Theoretical models of the chemistry have also been made. For example, Shields and Smith (Ref 18) and Shields et al. (Ref 19) have modeled the negative ion effects in CO_2 convection lasers and TEA CO_2 lasers, respectively. While these models provide some insight into the chemistry occurring in the discharge, they still rely on important assumptions regarding reaction rates. In many of the models, for example, the reverse reaction rates of most reactions were set equal to zero.

Review of Previous Studies

The experimental and theoretical studies of the plasma chemistry, some of which were mentioned in the last section, will now be discussed in detail. The results of each study will be given, and if applicable, a comparison with similar studies will be made.

In March 1969, Corvin and Corrigan (Ref 7) investigated the dissociation of CO_2 by electron impact in the positive column of a glow discharge. It was reported that from the measurement of the rate coefficients, the dissociation takes place via electron impact. The conclusion was that the dominant reaction is:

$$CO_2 + e^- \rightarrow CO + O + e^- \qquad (1.3)$$

Four months later, Gasilevich et al. (Ref 11) reported that

equilibrium for reaction (1.3) is reached in several seconds for large diameter discharge tubes and fractions of seconds in small ones. They went on to say that CO_2 dissociation becomes greater as pressure and flow velocity are decreased and discharge current is increased.

The following February, Buser and Sullivan (Ref 5) studied initial processes in CO_2 glow discharges. They reported that not only does collisional dissociation contribute to the CO_2 dissociation process as in reaction (1.3), but dissociative attachment as well. This dissociative attachment reaction is given by

$$CO_2 + e^- \rightarrow CO + O^- \qquad (1.4)$$

Buser and Sullivan also reported, for the first time, that H_2 in the mixtures reduces the dissociation process.

The experimental studies described so far, except the one by Corvin and Corrigan, involved a flowing gas system. In April 1970, Karube and Yamaka (Ref 12) investigated CO_2 dissociation in a non-flowing sealed CO_2 laser. Dissociation of CO_2 molecules was found to be consistent with the reaction

$$CO_2 \rightleftarrows CO + \frac{1}{2} O_2 \qquad (1.5)$$

with an equilibrium constant determined by the discharge parameters. For example, there was a 60% dissociation for a discharge current of 10 mA, and the dissociation increased slightly with increasing current.

Austin and Smith (Ref 2) identified the major positive ions in the total CO_2 laser mix and pure CO_2. The cathode region was sampled with a time-of-flight mass spectrometer, and the major ions for the total mix were CO_2^+, O_2^+, CO^+, N_2^+, and H_2O^+. The pure CO_2 discharge had the following ions: CO_2^+, O_2^+, CO^+, H_2O^+, O^+, and C^+. Although these results are valid in the negative glow and cathode fall regions, one should note that they may not necessarily be true in the positive column of the glow discharge where most of the laser excitation occurs. Austin and Smith published the results of their study in 1972.

In January 1973, Wiegand and Nighan (Ref 24) used a theoretical rate equation model and reported that numerous secondary minority species, such as those composed of carbon, oxygen, and nitrogen are produced in significant quantities on a time scale of 10^{-4} sec. The dissociation products CO and O are produced on the same time scale. These neutral minority species can reach concentrations in excess of the charged particle densities, and they are found to be directly related to the dominant ionic species. For typical laser discharge parameters, the negative ion species can become comparable to the electron concentration. The dominant negative ion species are CO_3^-, CO_4^-, NO_2^-, O^-, and NO_3^-. Shields and Smith (Ref 18) also reported five years later that in a typical

$CO_2/N_2/He/H_2O$ mixture, the principal ions are CO_3^-, CO_4^- and H^-. These negative ions are greater than ten percent of the electron concentration, but never exceed it. However, if the gases are recycled or if there is an air leak, the dominant negative ions are NO_2^- and NO_3^-. These ions can exceed the electron concentration. The results mentioned here are only applicable to CO_2 convection lasers. in TEA CO_2 lasers, Shields et al. (1976) stated that in Sealed $CO_2/N_2/He/O_2/CO/H_2/H_2O$ mixtures, the dominant ions are CO_4^- and H^-. However, in systems with little O_2 or H_2O added, the dominant ion is CO_3^- (Ref 19). The studies cited in this paragraph used a computer model of the plasma chemistry. Prince and Garscadden (1975) experimentally determined that NO_2^-, NO_3^-, O_2^-, O^-, and CO_3^- are indeed the principal negative ions formed (Ref 15). However, there is some discrepancy concerning the dominant negative ion. Prince and Garscadden found that the dominant negative ion is NO_2^- while the theoretical models predict CO_3^-. They did find that the CO_3^- concentration rises sharply at low discharge currents, and at higher currents, NO_2^- becomes the dominant negative ion.

Smith and Austin (Ref 20) continued the study of CO_2 dissociation in pulsed and continuous lasers in August 1973. This study measured CO_2 dissociation for a variety of E/p values. Important steps were made in studying CO_2 dissociation for a variety of mixtures with CO_2 as a

component. The dissociation is greater for $CO_2/N_2/He$ than for CO_2/N_2, and the dissociation is greater for CO_2/N_2 than for pure CO_2.

Thoenes and Kurzius expanded the research from CO_2 dissociation to the study of the plasma chemistry important in the formation of impurities (Ref 22). This study, done in August 1976, concentrated on closed-cycle CO_2 lasers. The two mixtures studied were $He/N_2/CO_2$ and $H_2/N_2/CO_2$. The study by Thoenes and Kurzius was again theoretical.

Two studies in November 1976 dealt mainly with positive and negative ion reactions in carbon dioxide, and ion-molecule reactions in CO_2 and CO_2/CO mixtures. These were done by Alger and Rees (Ref 1), and Coxon and Moruzzi (Ref 8), respectively. Alger and Rees reported that for pure CO_2, the dominant ions are O_2^+ and CO_2^+. They also measured the reaction rate for the following charge exchange reaction involving these ions:

$$O_2^+ + CO_2 \rightarrow CO_2^+ + O_2 \qquad (1.6)$$

Coxon and Moruzzi measured the rates for the formation of positive CO_2 cluster ions over a wide range of E/n values. The CO_2 cluster ion $(CO_2.CO_2)^+$ is formed by the following reactions:

$$CO_2^+ + 2CO_2 \rightleftarrows (CO_2.CO_2)^+ + CO_2 \qquad (1.7)$$

Other than the studies by Buser and Sullivan (Ref 5); and Smith and Austin (Ref 20), there has been no important

plasma synthesis study. This type of study will almost surely be advantageous in understanding plasma chemistry processes in CO_2 laser discharges.

Problem Statement and Approach

The present problem is to obtain an accurate picture of the plasma chemistry occurring in a CO_2 laser discharge. The "synthesis" approach, as described previously, will be used in order to reduce the ambiguity of the results. The neutral chemistry of the following mixtures will be studied experimentally by using a quadrupole mass analyzer: CO_2/Ar, N_2/Ar, CO_2/N_2/Ar, CO_2/He/Ar, and CO_2/N_2/He/Ar. The volume flow ratio of components in the multi-component mixtures above will reflect the same volume flow ratio found in typical CO_2 lasers (i.e., as in a 1:1:8 mixture of CO_2/N_2/He). A theoretical model of each mixture will be developed and compared to the experimental data.

II. Experimental Arrangement and Procedure

The complete mass analyzer system, not to scale, is shown in Fig. 1. The test gases were flowed through a discharge tube connected on-line to a quadrupole mass spectrometer. In the data acquisition system, there was no provision for automatic reduction of the data. The data reduction had to be done by hand calculation and with the aid of a computer. It is the purpose of this section to explain each of the parts of the total system shown in Fig. 1. The data reduction process is outlined in Appendix A.

Gas Handling System

A, B, C, and D in Fig. 1 represent the gas bottles where the four gases of this experiment were stored. These gases were CO_2, He, N_2, and Ar; and they were rated at a purity of 99.998%. The regulated flows were measured by Hastings mass flowmeters. The measured flows were accurate to ±1% for He and Ar, and ±5% for N_2 and CO_2. The entry of the gases into mixing manifold(E) was controlled by two valves: an on-off valve and a needle valve. The needle valve was used to control the flow rate of gases into the mixing manifold. The needle valves held much of the back pressure from the gas regulators, and this pressure was kept between 14.7 and 18 psi in order to

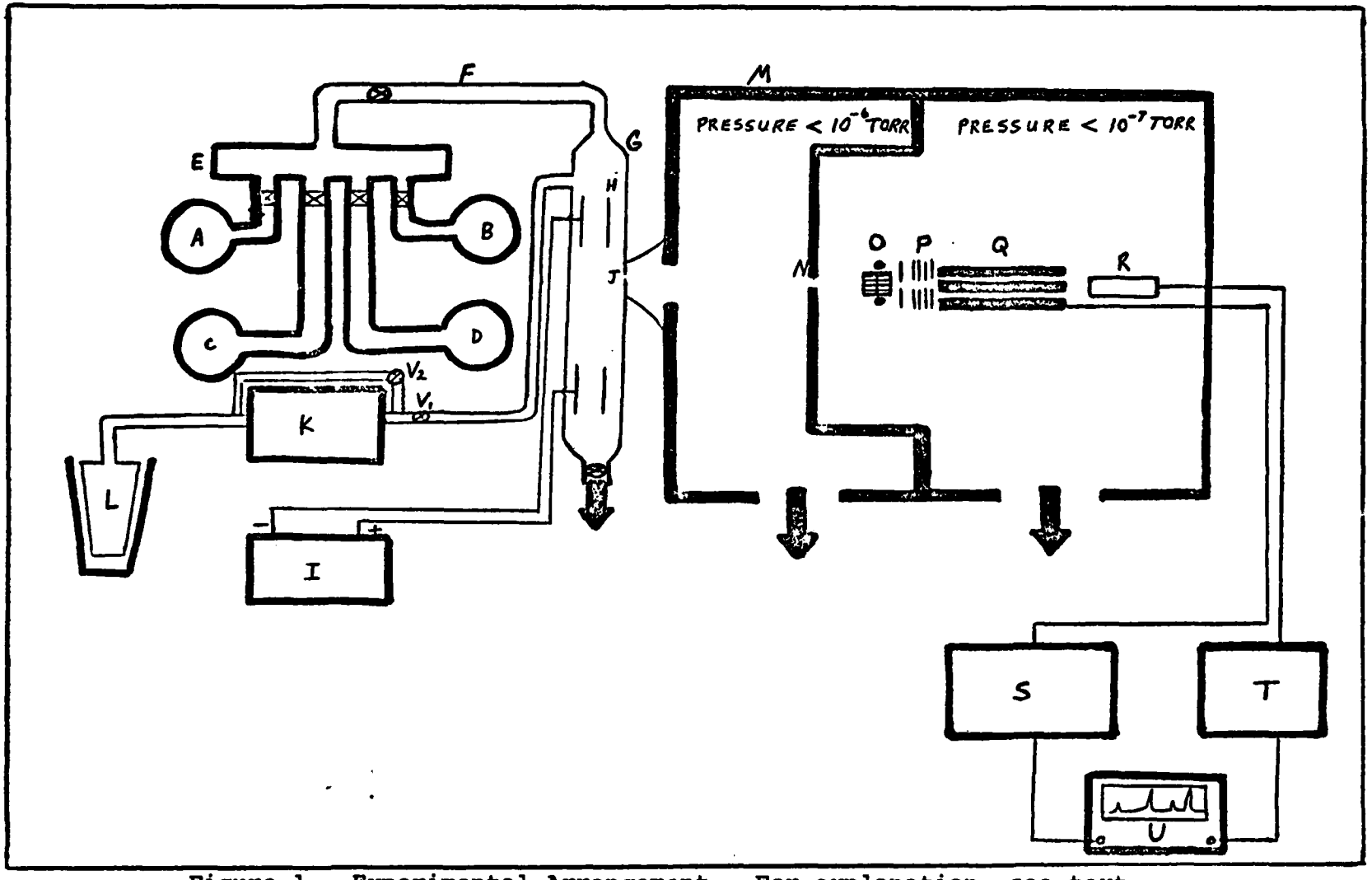

Figure 1. Experimental Arrangement. For explanation, see text.

avoid damage to these valves.

The mixing manifold consisted of a hollow cylinder. Normally, a packing of glass beads is used to aid in a thorough mixing of the gas components. In this experiment, glass beads were not imperative because of the slow flow used. The flow of each component gas in a mixture was less than 10 standard cubic centimeters per minute (SCCM), and the total flow was around 12 SCCM. At these slow flow rates, the gases have sufficient time in the glass tubing leading to the discharge tube (F in Fig. 1) to mix before entering the discharge tube itself (G in Fig. 1). The mixing was also aided by the low pressure used in the experment (2 torr). This is not the case for very high flow rates. Another advantage of a slow flow is that the total flow rate of a mixture of gases is just the sum of the flow rates of the individual components.

The Discharge Tube

The discharge tube (G) was of pyrex construction with an outer jacket for cooling water. The inner diameter was 2.50 cm, and the length was approximately 30-40 cm. The hollow cylindrical electrodes (H), which were separated by a distance of 30 cm, were made of Kovar.

The discharge was controlled by a current regulated high voltage power supply (I), and the cathode of the discharge tube was located upstream of the gas flow. The maximum current attainable was around 80 mA. In a N_2/Ar

discharge, arcing occurred at about 70 mA. The sampling orifice (J) was located midway between the two electrodes so that it sampled from the positive column of the glow discharge. The orifice used in this experiment was 2 mils in diameter. The residence time (see Appendix B) is the length of time that a portion of the gas stays in the discharge before it is sampled by the spectrometer. It is given by

$$\tau = \frac{A\ell p}{Hp_a} \qquad (2.1)$$

where A is the cross-sectional area of the discharge tube, ℓ is the length from the cathode to the sampling orifice, p is the pressure of the gas, p_a is the standard pressure (760 torr), and H is the total flow rate given in SCCM. The residence time for this experiment was chosen to be 1 sec. This choice permitted a flow that was measurable by the flowmeters. Once a residence time is chosen, a restriction is made on the total flow rate H for a particular gas pressure p. Solving for H in equation (2.1) and using the parameters that are applicable to this experiment (i.e., ℓ=15cm, A=πa^2 where a is the inner radis of the discharge tube, and τ=1sec), the flow rate is

$$H = (5.81)p \qquad (2.2)$$

The pressure in the discharge was measured by a differential capacitance manometer (K) manufactured by MKS

Instruments, Inc. All pressure measurements were made upstream of the gas flow behind the cathode of the discharge tube. The reference pressure was obtained via a cold trap (L) at liquid nitrogen temperature. The procedure for obtaining the reference pressure is as follows. First, the manometer head and cold trap are pumped down by the same forepump that evacuates the discharge tube. To do this, valves V1 and V2 are opened. Next, valve V1 is closed and the cold trap is filled with liquid nitrogen. Now the manometer is at the pressure of the cold trap, and the meter is zeroed. To measure the pressure of the discharge tube relative to the cold trap pressure, valve V2 is closed and V1 opened. It is important to keep the cold trap filled with liquid nitrogen. If the trap is allowed to increase in temperature, then the reference pressure changes which results in a change in measurement of the source pressure.

The Quadrupole Mass Spectrometer

The spectrometer used in this experiment was a quadrupole mass filter manufactured by Extranuclear Laboratories, Inc. The model is an EMBA II. The molecular species to be analyzed are first ionized before detection. The complete mass spectrometer system is designated M in Fig 1. There are two differential pumping stages. The first is pumped by a turbomolecular pump, and the second by a diffusion pump. The first stage is usually pumped down to

a pressure of 2.4×10^{-7} torr while the second stage to a pressure of 8.4×10^{-8} torr. The molecular beam from the orifice is chopped by an electric tuning fork chopper before entering the rear orifice (N). This chopped beam is then ionized by the ionizer (O), and the resultant ion beam is focused by a series of lenses (P) before entering the quadrupole region (Q).

The lens system consists of a lens to control the ion energy, an extractor, and three focusing lenses. The first lens is given a positive potential, and only positive ions of a certain minimal kinetic energy can surmount the potential barrier. The extractor is given a negative potential to accelerate the ions toward the focusing lenses. The three focusing lenses are given potentials (positive or negative) to focus the ion beam into the quadrupole region (Q).

Theory of Quadrupole Mass Filtering. The most complete theory of quadrupole mass filtering is given by P[illegible] et al. (Ref 14). However, the following summary is adapted from Ref 16. Four symmetric hyperbolic electrodes, described by the equation $X^2-Y^2 = \pm C$ where C is a constant, make up the quadrupole mass filter. Two opposite electrodes are given the potential $\phi(t) = U+V\cos(\omega t)$, where U is a dc voltage and V is the peak amplitude voltage of a radio-frequency source of angular frequency ω. The other two electrodes are given the same potential, but of opposite

sign of the first two. Fig. 2 shows this configuration. Under these conditions, a quadrupole field is set up with the field on axis equal to zero.

If an ion is injected with a velocity parallel to the z axis, it undergoes a transverse motion. The equations of motion in the xy plane are given by Mathieu equations, and the solution is either exponential or oscillatory. For a given U and V, ions of a particular q/m will have stable trajectories through the quadrupole assembly. This stable trajectory consists of oscillatory motions about the z axis coupled with a velocity parallel to the z axis such that the particle does not strike the electrodes. Since the pressure in the back chamber of the spectrometer is less than 10^{-7} torr, the mean free path of the ions is great enough so that collisions among ions are negligible when undergoing the oscillatory motions. All ions without the right q/m value will ultimately strike the electrodes and be removed from the ion beam. The mass resolution is given by

$$\frac{m}{\Delta m} = \frac{0.126}{0.16784-U/V} \qquad (2.3)$$

Note that the resolution of the mass filter can be varied by varying the ratio U/V. If U/V = 0.16784, then a theoretical infinite mass resolution is achieved. For infinite mass resolution,

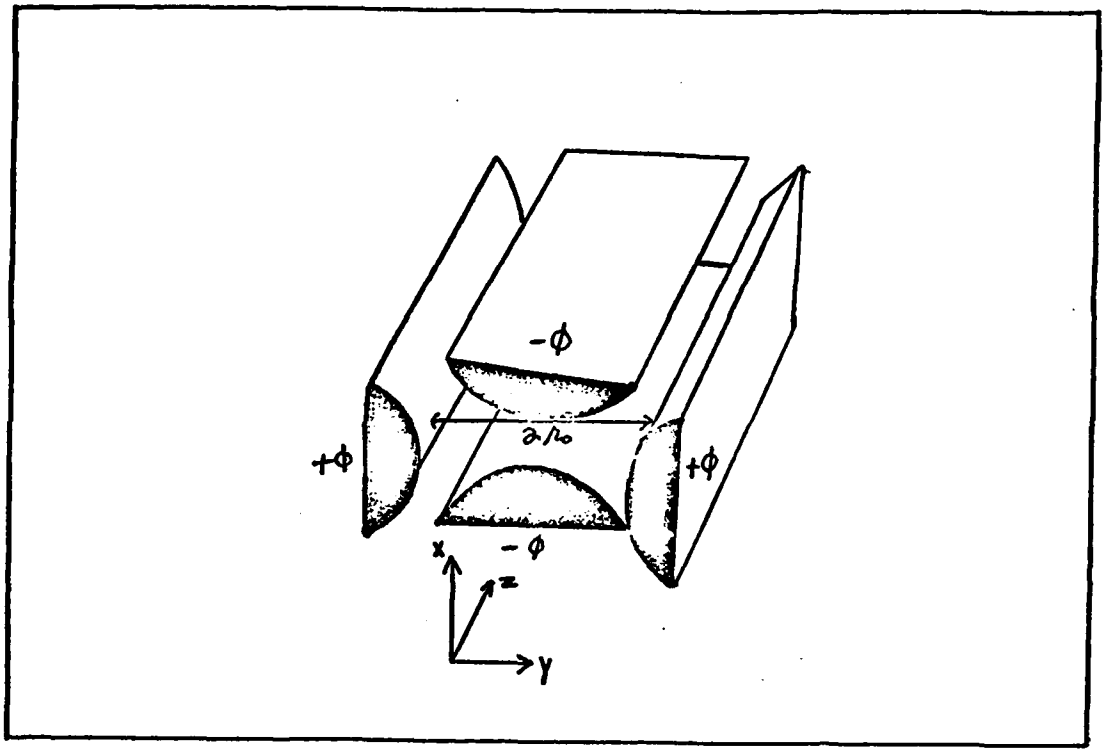

Figure 2. Quadrupole Mass Filter

$$U = 1.212\ mf^2 r_o^2 \qquad (2.4)$$

$$V = 7.219\ mf^2 r_o^2 \qquad (2.5)$$

where m is the mass in amu, f is the frequency of the rf source in MHz, and r_o is the radius of the circle inscribed tangent to the four hyperbolic electrodes (see Fig. 2).

In order for mass separation to occur, the ion of the incorrect q/m must stay in the quadrupole long enough so that it can be filtered out. Hence, this requirement puts a restriction on the ion energy and length L of the electrodes. The approximate relationship is given by

$$E_{ion} < \frac{1}{25} f^2 L^2 \left(\frac{\Delta m}{m}\right) m \qquad (2.6)$$

where E_{ion} is the kinetic energy of the ion in eV, and L is the length of the quadrupole assembly given in cm. Lighter ions will be transmitted more than heavier ions because of their greater velocity. Although lighter and heavier ions may have the same kinetic energy, their respective velocities through the quadrupole are different. Therefore, there is a transmission discrimination against heavier ions. To compensate for this, the ion energy control may be increased with increasing mass units. The spectrometer used in this experiment did not have the provision of increasing ion energy with increasing mass units.

There is also a maximum aperture radius of ion injection into the quadrupole region. If the ion is injected too far off from the z axis, it will strike the elctrodes even if it has the correct q/m. For ions injected parallel to the z axis, the maximum aperture radius of ion injection to insure that none will strike the electrodes is given by

$$a \approx \frac{2}{3} r_o \left(\frac{\Delta m}{m}\right)^{\frac{1}{2}} \qquad (2.7)$$

From equations (2.3), (2.6) and (2.7); it is evident that the resolution and transmission of the ions through the filter can be controlled by varying the applied voltages U and V. The achievement of good resolution and transmission depends on the stability of these two voltages. The quadrupole mass filter used in this experiment has provisions for adjusting the resolution and transmission

by varying the ratio of the two voltages. Also, it can be seen from equations (2.4) and (2.5) that mass selection can be done by either varying U and V, or f. In the Extranuclear quadrupole system, U and V are varied while f is held constant. Therefore, the two voltages, U and V, play an important role in ion transmission and mass discrimination.

Particle Detector. All Extranuclear particle detectors are designed so that the first dynode is not on axis with the mass filter. The particle detector is denoted by R in Fig. 1. This arrangement prevents photons and neutrals from striking the first dynode producing random noise in the electronics. The paraxial detector, in which the multiplier is offset but parallel to the axis of the quadrupole, is used in the EMBA II mass spectrometer.

After exiting the mass filter, the ions enter a space in which the surrounding walls are at ground potential (i.e., the spectrometer case is grounded). The partition that separates the mass filter from the particle detector contains a circular aperture which approximately matches the viewing area of the first dynode of the particle multiplier. The first dynode is usually kept at a high negative voltage so that the ions are drawn to it. The multiplier voltage was kept at -4 kV in this experiment.

Quadrupole Controls. The quadrupole control unit (S in Fig. 1) serves several functions. Circuitry is

provided to control the voltage output of U and V to a fixed value. U and V may also be swept over certain ranges with the aid of a sweep generator; and the sweep is over a specified range of m/q. The output of the sweep was connected to the x input of the x-y plotter. There are also provisions for indicating the value of m/q that the quadrupole is tuned to. The resolution mode can be varied by letting $U=\gamma V-\delta$ in equation (2.3) where γ and δ are constants. The constants γ and δ can be controlled, and these are the resolution and Δm controls, respectively. The resolution was set at a ratio of 8.15, and the Δm was set at +1.8 volts. These settings eliminated peak splitting in the output sweep. Another control to improve peak shaping is called the pole bias; and this control was set at -0.4 volts which improved the symmetry of the peak. The resolution, Δm, and pole bias controls depended somewhat on the size of the signal and sensitivity setting.

Detection Electronics

The detection electronics consisted of a particle multiplier, lock-in amplifier, and an x-y plotter. These parts are schematically represented by R, T, and U in Fig. 1. The particle multiplier has been discussed in some detail in a previous section. As stated earlier, a tuning fork chopper is located in front of the second aperture to the back chamber of the spectrometer. This chopper chopped the molecular beam, thus providing a modulated

signal to the particle detector. The signal from the particle detector was fed to the lock-in amplifier with the frequency of the tuning fork as a reference. The signal output from the lock-in amplifier was then led to the y input of the x-y plotter.

The settings on the amplifier and x-y plotter were kept the same on all spectra with the exception of an increase in amplifier sensitivity on some. The time constant of the amplifier was 300 ms, and the sensitivity was 5 mV on the following spectra: CO_2/Ar, N_2/Ar, and $CO_2/N_2/Ar$. The spectra of those mixtures which contained helium were taken at a sensitivity of 2 mV. The 2 mV sensitivity was used on the following mixtures: $CO_2/He/Ar$ and $CO_2/N_2/He/Ar$. This higher sensitivity produced a recognizable helium signal. The period of the sweep on all recorded spectra was 300 sec.

Special Calibrations

Aside from the instrumentation calibration given in the EMBA II manual, there are two important non-instrument calibrations that must be made. These are the contact potential offset of the ionizer energy meter and the spectrometer function. Both of these calibration factors play an important role in the data reduction process (see Appendix A). These factors will be discussed in some detail below.

Contact Potential. The energy reading from the meter

is not the energy of the ionizing electrons. The meter reading is just the potential difference between the filament and grid, but the energy of the electrons is actually distributed about this value. Aside from this fact, there is an electron energy offset between the ionizer and the meter due to the connections between the two. It is a well known fact that there is a contact potential difference between two dissimilar metals connected together. This potential difference is expected to be on the order of a few volts.

To determine this contact potential, appearance potential plots are run for different gases. The difference between the reading from the plot and the actual appearance potential is the amount of offset. In this experiment, appearance potential plots were run for CO_2, N_2, He, and Ar. The offset was approximately 3.5 volts. This voltage offset also takes into account the effect of the space charge of the ionizer and the energy loss in overcoming the work function of the cathode.

Spectrometer Function. The mass spectrometer used in this experiment is a number density measuring device. As stated earlier, the test gas is first ionized before detection. Fig. 3 shows the construction of the ionizer. The sample molecular beam is led into the cylindrical grid where it is crossed by an electron beam. It is constructive at this point to derive an expression for the total ion

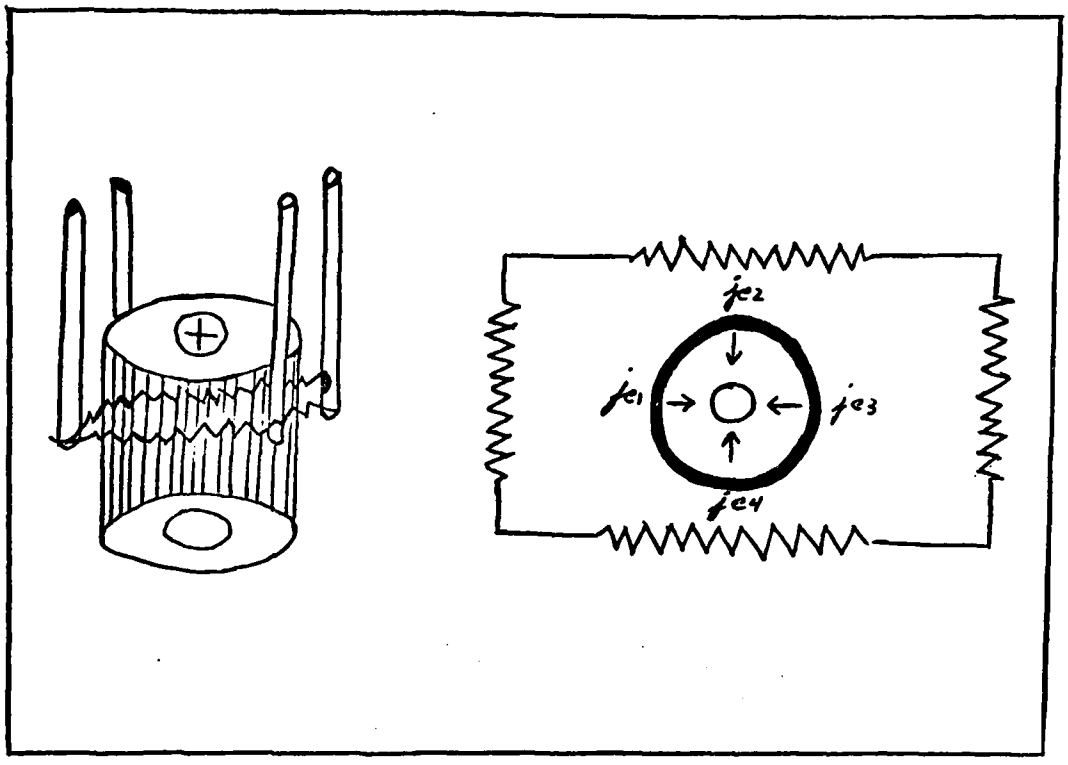

Figure 3. Electron Impact Ionizer

current density that is formed by the ionizer. Out of this expression, the spectrometer function will be defined. The simplified ionizer shown in Fig. 4 will be considered in the following analysis.

The number of ionizing collisions per unit volume per unit time between electrons and molecules is given by

$$\dot{n} = n_e n_s < V\sigma_s(V) > \qquad (2.8)$$

where

n_e = the electron number density

n_s = the molecular number density of molecular species s

V = the magnitude of the relative velocity

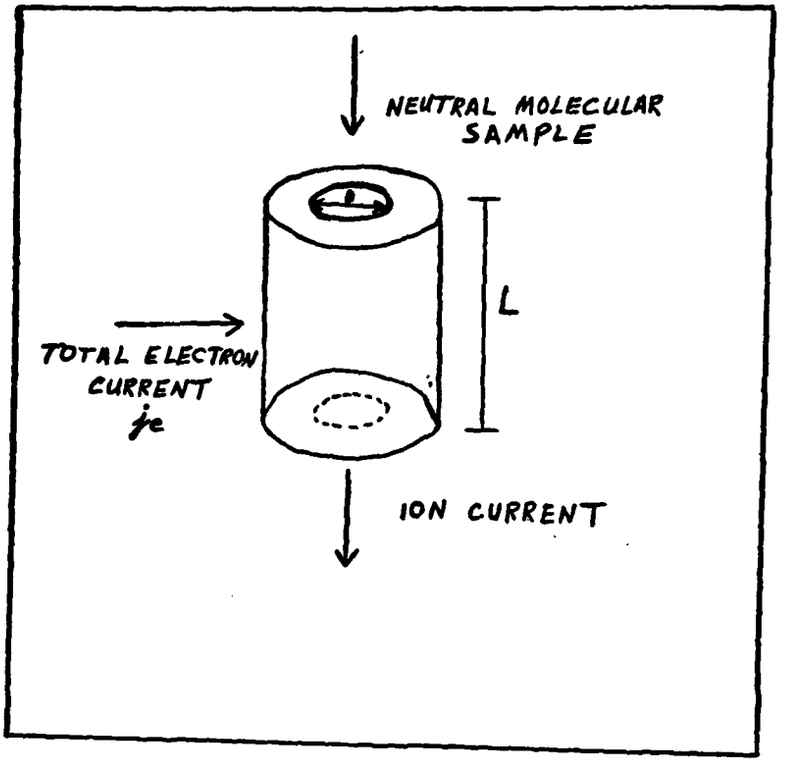

Figure 4. Simplified Ionizer

$\sigma_s(V)$ = the total ionization cross-section of molecular species s

The <> denotes a calculated average in velocity space of the product $V\sigma_s(V)$.

It is assumed that the electrons possess most of the kinetic energy such that $V \simeq V_e$ where V_e is the speed of the electrons. It is further assumed that the speed of the electrons is constant. Therefore, equation (2.8) reduces to

$$\dot{n} = n_e n_s \sigma_s V_e \qquad (2.9)$$

The magnitude of the interacting electron current density in the ionizer is assumed to be given by

$$j_e = q_e n_e v_e \tag{2.10}$$

where q_e is the magnitude of the electronic charge. That is, the assumption has been made that the ionization process is not having to compete with other processes such as inelastic scattering, dissociation, etc. Solving for n_e in equation (2.10) and substituting into equation (2.9), the following result is obtained for the number of ions per unit volume per unit time formed by the ionizer:

$$\dot{n} = \left(\frac{j_e}{q_e}\right) n_s \sigma_s \tag{2.11}$$

The number of ions formed per second in the ionizer is obtained by multiplying equation (2.11) by the volume of the interaction region:

$$N = \frac{\pi}{4} D^2 L \dot{n} = \frac{\pi}{4} D^2 L \left(\frac{j_e}{q_e}\right) n_s \sigma_s \tag{2.12}$$

where D is the diameter of the entrance aperture and L is the length of the ionizer (see Fig. 4). If these ions are now swept out as fast as they are produced, then the ion current density becomes

$$j_s = \frac{q_s N}{\pi/4D^2} = \left(\frac{q_s}{q_e}\right) j_e L \sigma_s n_s = j_e L \sigma_s n_s \tag{2.13}$$

Equation (2.13) states that the extracted ion current density

is proportional to the product of the molecular number density and total ionization cross-section of molecular species s. Equation (2.13) also assumes that the molecules are singly ionized.

When the quadrupole is tuned to a particular mass number, the signal is proportional to equation (2.13).

$$(PH)_s = (C_s j_e L)\sigma_s n_s \qquad (2.14)$$

where $(PH)_s$ stands for the signal measured in terms of the deflection of the chart recorder, and C_s is a constant of proportionality. C_s is in general different for each molecular species. Equation (2.14) defines what is known as the spectrometer factor. The spectrometer factor is given by

$$F_s \equiv C_s j_e L \qquad (2.15)$$

Using the definition of the spectrometer factor, equation (2.14) becomes

$$(PH)_s = F_s \sigma_s n_s \qquad (2.16)$$

The factors in equation (2.15) describe certain characteristics of the spectrometer. These factors will be discussed in some detail below.

The electron current density (j_e) and the length of the interaction region (L) are both characteristics of the ionizer. The electron current density of the ionizer depends on the rate of thermionic emission from the filament,

and it also depends on the potential difference between the filament and the grid. The interaction length is just the length of the ionizer.

C_s includes the characteristics of the particle multiplier and detection electronics. The response of the particle multiplier is a function of the number density and impact energy of the atoms or molecules of a particular species. In the effusive flow regime, the velocity distribution of the molecules is Maxwellian. Although a flowing gas mixture is used in this experiment, it is assumed that the velocity distribution of each species is still Maxwellian about a coordinate frame moving with the same velocity as that of the gas. The response of the particle multiplier will be the same for all species with the same mass number if equal number densities of these species strike the particle multiplier. In the regime of a free-jet expansion, the molecules reach a terminal velocity at a point of about 30D where D is the diameter of the orifice (Ref 22:12). This terminal velocity is given by

$$V = ((2\gamma/\gamma-1)(kT_s/m))^{\frac{1}{2}} \qquad (2.17)$$

where m is the molecular mass, T_s is the temperature of the source, k is Boltzmann's constant, and γ is the ratio of the specific heat at constant pressure to that at constant volume. If the flow contains a mixture of gases, then V is the mass average velocity and m is the average mass. The ratio of the specific heats, γ, is just that of the

mixture. Therefore, molecular species in a mixture have the same terminal velocity. Again the signal is the same for all molecular species with the same mass number (if their number densities are equal). It should be noted that while two molecular species may have the same mass number, their internal degrees of freedom may be different. The number of secondary electrons emitted by the first dynode of the particle multiplier depends on the total energy which is the sum of the translational and internal energies. Therefore, it is assumed that the internal energy is negligible compared to the translational energy in order to simplify the data reduction process. This is a valid assumption since ions are accelerated by the high negative voltage of the first dynode.

There are advantages and disadvantages to both of the flow regimes described above. While a correct picture is given of the chemical makeup of the source in the effusive flow regime, the sensitivity of the detection electronics must be high in order to obtain recognizable signals. This high sensitivity is required due to the weak intensity of the molecular beam. The free-jet expansion is advantageous in producing a high intensity beam, but it has the disadvantage of altering the original chemistry of the source. The reason is that a free-jet expansion is collision dominated, and chemical reactions are bound to occur within the beam before detection. The most desirable flow regime is neither effusive nor free-jet expansion,

but a transition flow which is between the two. However, any predictions concerning transition flow are limited to the analytical models of effusive flow and free-jet expansion. There is little knowledge to date concerning the regime of transition flow.

The number density, n_s, in the ionizing region of the ionizer obviously depends on the partial pressure of molecular species s in the source. If the molecular beam consists of a mixture of gases, then diffusive separation can occur (Ref 17). The factor C_s also takes into account this diffusive separation of components in the beam. Moreover, it will be assumed that the fractional amount of the total number density of each component in the beam is the same as that in the source.

When F_s is solved for in equation (2.16), the following result is obtained:

$$F_s = \frac{(PH)_s}{\sigma_s n_s} \tag{2.17}$$

A plot of F vs. atomic mass unit is known as the spectrometer function. To generate points for this plot, different gas mixtures are flowed individually through the discharge tube with the number density of each molecular species known. From the experimentally determined signal, and the known ionization cross-section corresponding to the energy of the ionizer, an F corresponding to the atomic mass unit of each molecular species can be found. The

accuracy of the plot is increased if several individual gases are used.

Fig. 5 shows a plot of F vs. atomic mass unit. The following gases were used to obtain this plot by using the method described in the previous paragraph: H_e, N_2, Ar, and CO_2. The electron energy of the ionizer was set at 70 eV. In equation (2.17), $(PH)_s$ is in units of cm (i.e., the deflection in cm of the chart recorder) and σ_s is in atomic units (πa_o^2, where a_o is the Bohr radius).

A close examination of equation (2.17) indicates that F is highly dependent on the partial pressure of molecular species s in the source. The reason for this dependency is that the number density in the molecular beam increases with an increase in partial pressure and vice versa. Under a discharge current of 80 mA, the pressure increases by as much as 0.4 torr in CO_2/Ar. F is assumed not to change much for this small increase in pressure due to the discharge.

From the arguments given in the Spectrometer Characteristics section concerning the constant of proportionality C_s, it is not unreasonable to assume that F is the same for all atomic or molecular species with the same or nearly the same mass number. This assumption allows an F to be read for any additional molecular species produced in the discharge from a predetermined plot. Because of the large dispersion shown in Fig. 5, F should be calculated separately for each species in the cold gas mixture

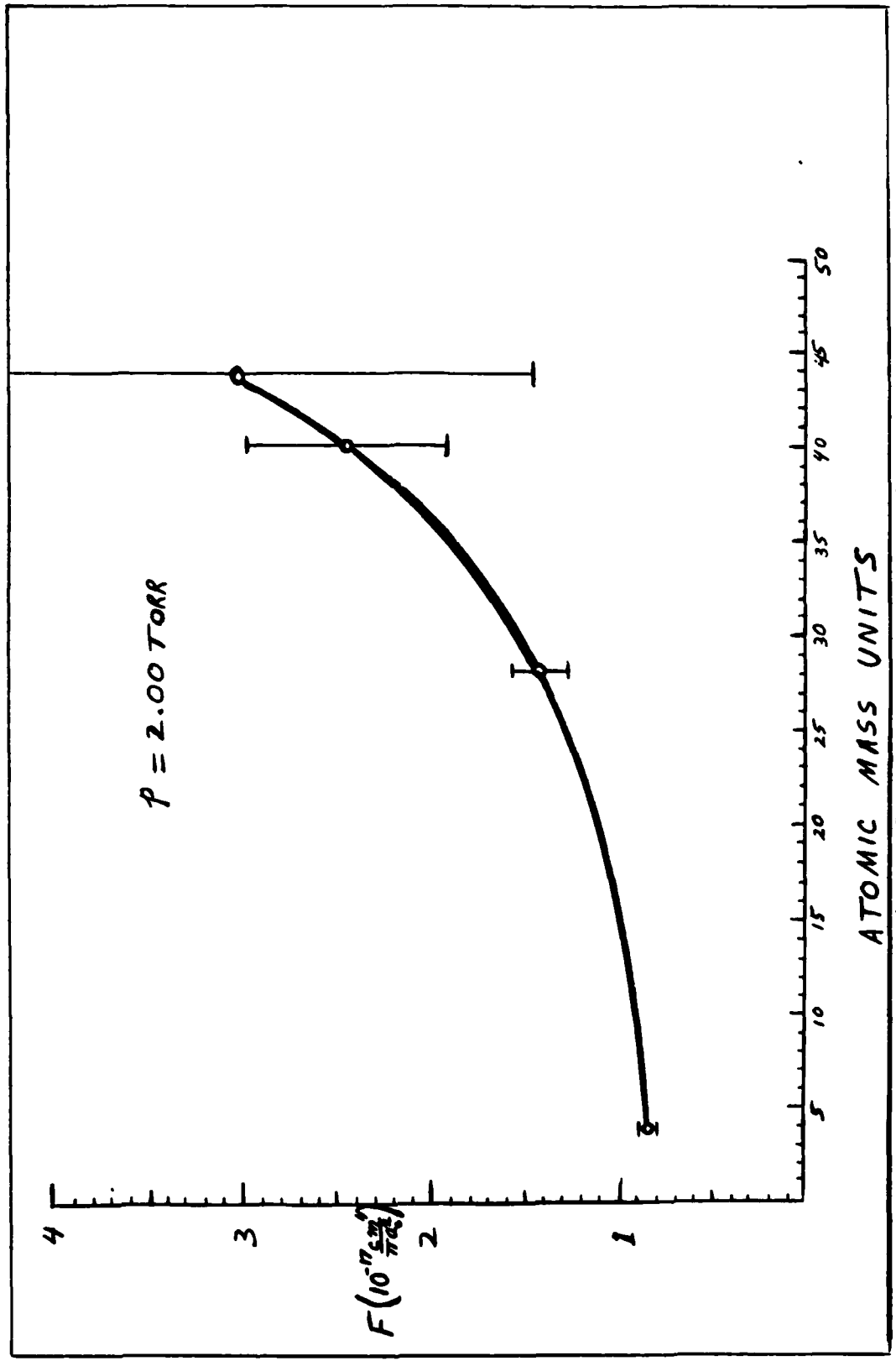

Figure 5. Spectrometer Function

and used in the reduction process. The curve in Fig. 5 should only be used to obtain an F for the additional molecular species produced in the discharge.

III. Experimental Results

The experimental results of the mixtures considered in this experiment will be given in this section. In all of the mixtures, the amount of Ar was 10% in order to monitor the density changes during the discharge. The voltage and pressure effects of the discharge are first discussed. Afterwards, the neutral chemistry of the mixtures will be presented. Where possible, a comparison will be made with other similar experiments in the literature.

Voltage Effects

Fig. 6 is a plot of discharge voltage vs. current for all of the mixtures. The sustaining voltage of the discharge depends on many factors. As evident from Fig. 6, it depends on the particular gas mixture. Other factors include ionization cross sections, the reduced field (E/n), and the ionization efficiency. Arcing occurred in the N_2/Ar discharge above a discharge current of approximately 75 mA. One reason for the high voltage of the N_2/Ar discharge is that the ionization efficiency of N_2 is low compared to the other gases used in this experiment.

Pressure Effects

The pressure in the discharge tube was 2 torr for all the mixtures before the discharge was turned on. After

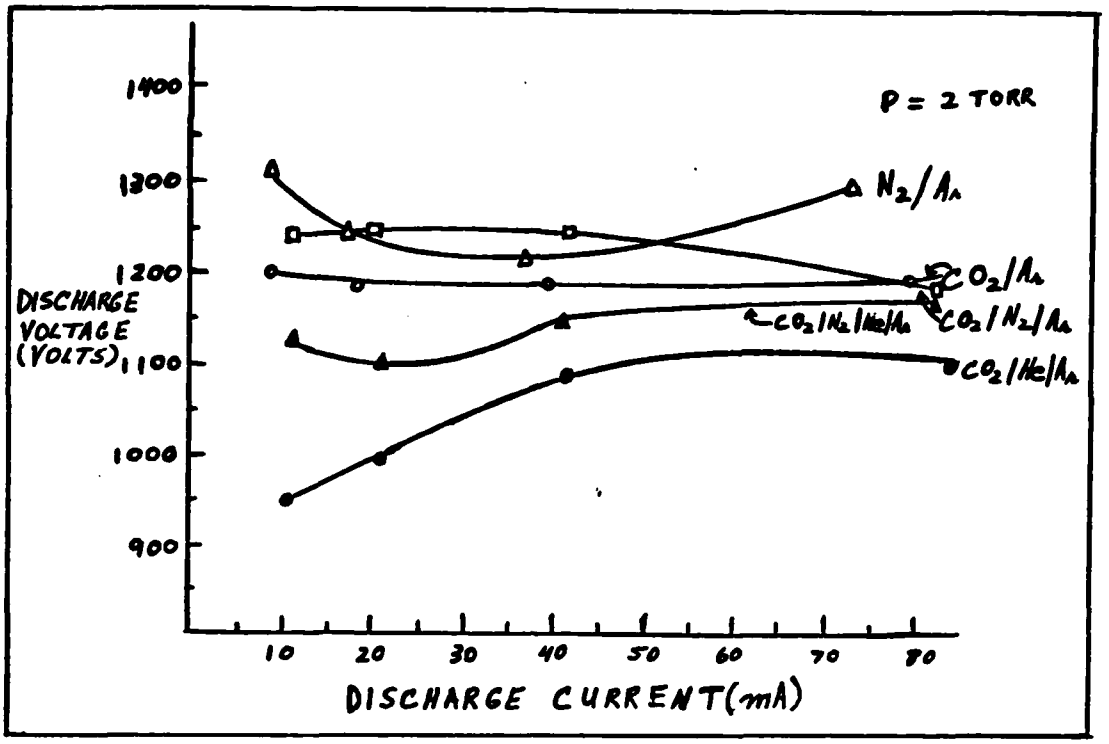

Figure 6. Discharge Voltage Vs. Current of Experimental Mixtures

the discharge was turned on, the pressure increased in CO_2/Ar, CO_2/N_2/Ar, CO_2/He/Ar, and CO_2/N_2/He/Ar; but decreased by one-one hundreth of a torr in the case for N_2/Ar. This pressure decrease has also been observed by Karube and Yamaka (Ref 12:2036). The pressure increase is due to the formation of new species in the discharge and/or gas heating.

Fig. 7 shows the effect of the discharge on the source pressure. The curves for CO_2/Ar, CO_2/N_2/Ar, CO_2/He/Ar, and CO_2/N_2/He/Ar exhibit the same shape as the experimental curves indicating the rise in dissociation products as a function of discharge current. The buildup of certain species as a function of discharge current will be shown

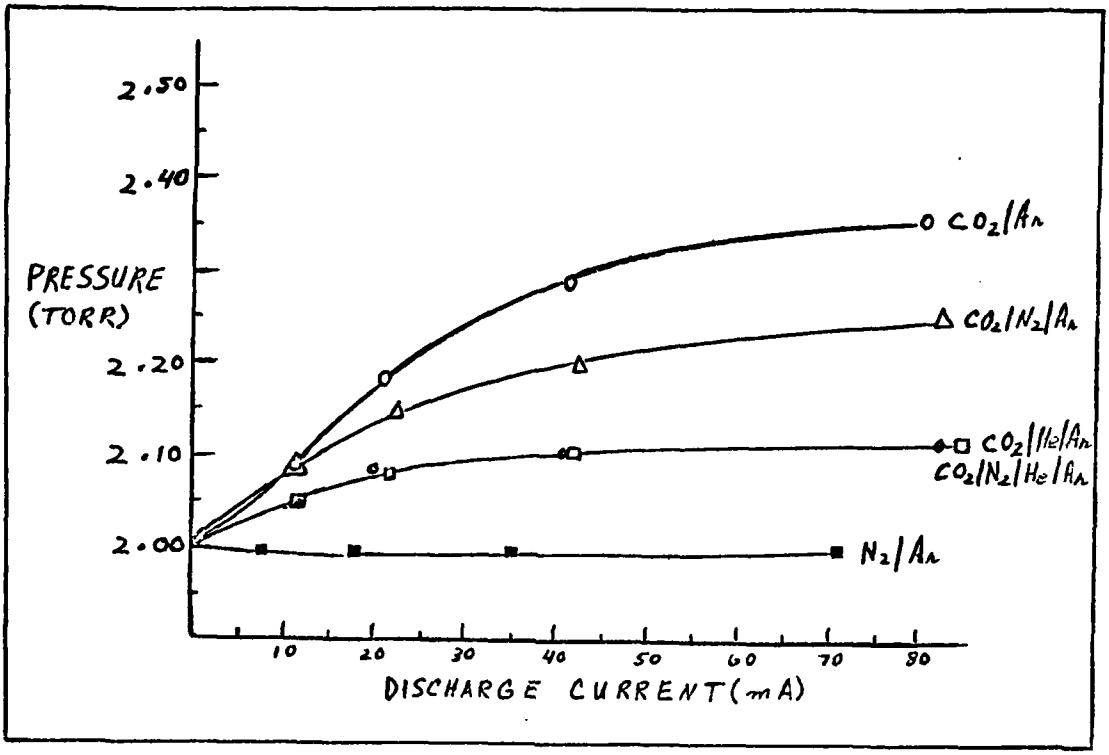

Figure 7. Pressure Vs. Discharge Current of Experimental Mixtures

later in this section. Therefore, it is concluded that the pressure effects were predominantly due to the formation of secondary species.

Further support is given to this conclusion by noting the curve for N_2/Ar in Fig. 7. Experimentally determined in this thesis, there is little dissociation in a N_2/Ar discharge. If the conclusion that the rise in source pressure was due primarily to the formation of secondary species is valid, then the curve for N_2/Ar is entirely consistent with this conclusion. Moreover, the pressure rise in N_2/Ar should be greater than the other mixtures if gas heating was the cause (i.e., the N_2/Ar discharge is very hot and the pressure should rise dramatically).

90% CO_2/10% Ar

Fig. 8 summarizes the chemistry of a CO_2/Ar discharge. Initially with a CO_2 concentration of 90%, the amount of CO_2 dropped rapidly with discharge current until a current of about 50 mA was reached. The number of CO_2 molecules dissociated was greater in a CO_2/Ar discharge than in any other mixture considered in this experiment. The fractional dissociation was up to 44%. Buser and Sullivan have shown that dissociation up to 80% is common (Ref 5:479).

This large dissociation can be explained by the following. Smith and Austin reported in 1974 that dissociation is preceded by the production of an excited state of CO_2 by electron impact (Ref 20:321):

$$CO_2 + e^- \rightarrow CO_2(^3\pi) + e^- \qquad (3.1)$$

Subsequent dissociation occurs though the following reaction:

$$CO_2(^3\pi) + e^- \rightarrow CO + O + e^- \qquad (3.2)$$

Shields et al. (Ref 19:1589) gave the overall rate constant for this dissociation mechanism as 1×10^{-9} cm^3s^{-1} (300°K). This rate is considerably larger than the rate for dissociative attachment:

$$CO_2 + e^- \rightarrow CO + O^- \qquad (3.3)$$

which has a rate constant at 300K° of 5×10^{-13} cm^3s^{-1} (Ref 19:1589). In a predominantly CO_2 discharge, there are

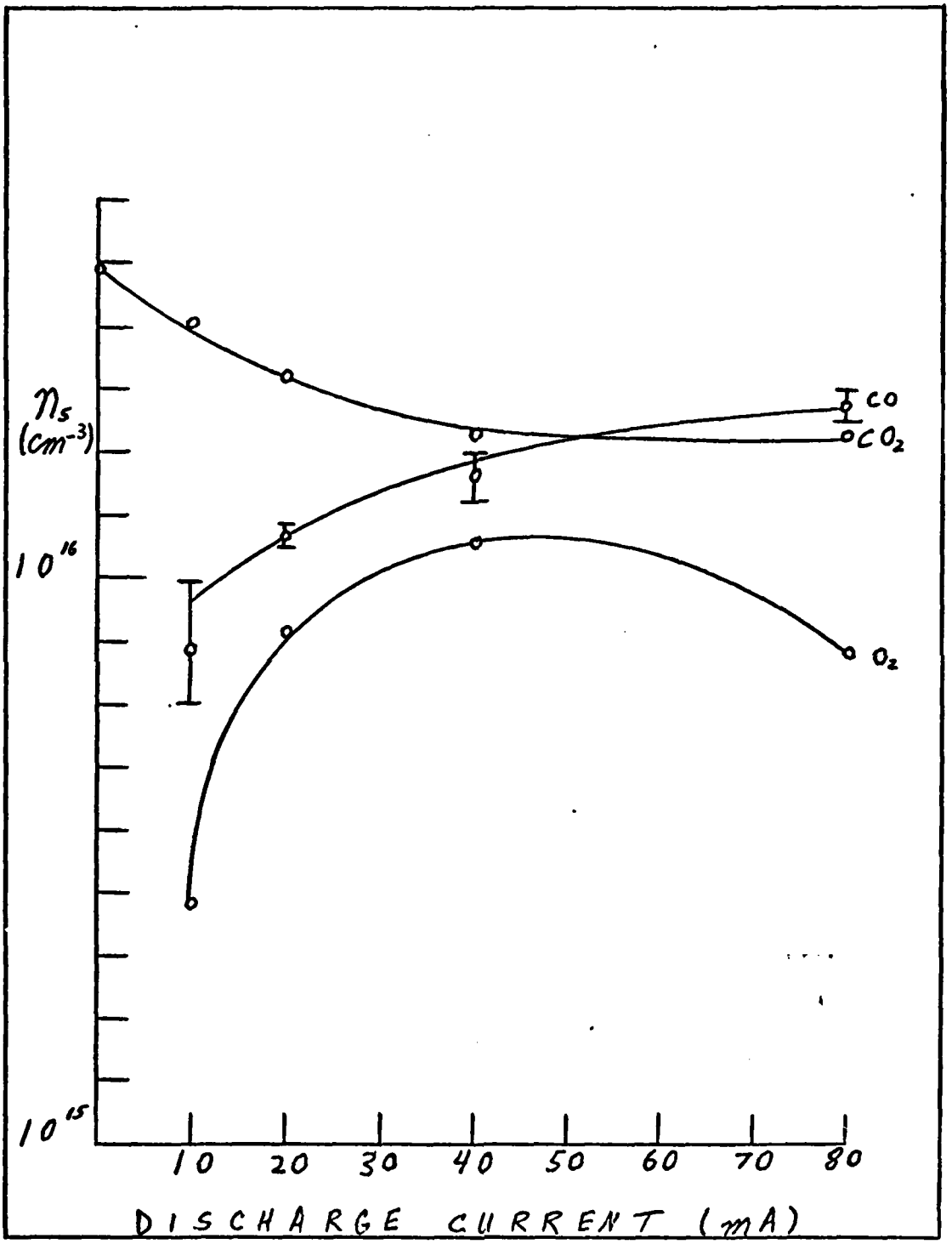

Figure 8. Number Density Vs. Discharge Current of the Major Species in a 90% CO_2/10% Ar Discharge (Experimental)

more interactions between electrons and CO_2 molecules than mixtures containing CO_2 in which the other components are comparable to the CO_2 percentage. Thus, there are more CO_2 molecules in the $^3\pi$ state and subsequent dissociations through reaction (3.2).

At a current of 80 mA, the CO percentage was about 55%. This is consistent with the 44% dissociation of the CO_2 as noted earlier. The rise in CO percentage was considerably higher in CO_2/Ar than in the other mixtures. The apparent reason is the same as that given above.

The dispersion of the experimental CO data points is inferred from the dispersion of the spectrometer factor given in Fig. 5. Since the CO_2 was an initial component in all experimental mixtures, a spectrometer factor was obtained for it in the cold gas and used in the reduction of the CO_2 percentage. Hence, dispersion in the CO_2 percentage cannot be determined. Dispersion in the O_2 percentage cannot be determined because the spectrometer factor for O_2 was not taken from actual experimental data, but from the curve in Fig. 5. Therefore, the dispersion in percentage can only be given in the case of CO.

The only explanation offered for the decrease in O_2 at high currents is that at a current of 50 mA, the dissociation of O_2 occurs. With the dissociation of O_2, the percentage of atomic oxygen should increase. Atomic oxygen should be readily detectable (Ref 5:474); however, none was detected in the CO_2/Ar discharge. Furthermore, 0 was

not detected in either of the mixtures studied in this experiment. Two mechanisms may contribute to the loss of atomic oxygen. First, the recombination of atomic oxygen on the walls of the discharge tube to form O_2 is occurring. The rate constant for such a process depends on the diffusion of O to the walls. Secondly, the adsorption of O to the walls and sampling orifice of the mass spectrometer is also a possible mechanism by which O is lost. However, not all of the atomic oxygen is lost by the two processes above. The remaining O in the discharge that did not recombine or get adsorbed may be below the sensitivity of the spectrometer.

Ozone may also be present, but was not detected. Increasing the sensitivity of the spectrometer to observe O and O_3 increases the background noise of the detection electronics causing the O and O_3 signals to be indistinguishable. To prove that O and O_3 are present in the discharge, spectroscopic techniques must be employed.

<u>90% N_2/10% Ar</u>

There was no detectable dissociation of N_2 in a N_2/Ar discharge. This conclusion is based on the fact that there was no rise in the N signal and no change in the N_2 signal. This conclusion is also supported by the pressure effects of the N_2 discharge as shown in Fig. 7. An increase in pressure would indicate the formation of additional species, but no such increase is evident from the N_2/Ar curve in Fig. 7.

Since there was no measurable dissociation, it is interesting to know where most of the power (possessed mainly by the electrons) from the discharge was transferred. Below an E/n of 10 x 10^{-16} Vcm^2, most of the power is transferred to vibrational excitation. Above 10 x 10^{-16} Vcm^2, most is transferred to exciting the electronic metastable state of N_2 and total electronic excitation. The plot for fractional power transferred in N_2 vs. E/n is given in Fig. 9.

The electric field in the positive column of a N_2/Ar glow discharge can be calculated approximately in the following way. By knowing the material composition of the electrodes, the cathode fall of potential in volts can be determined. The composition of the electrodes was Kovar, and for a N_2 discharge the cathode fall is on the order of 200 V (Ref 23:229). From Fig 6, the maximum and minimum tube voltages were 1300 and 1250 V respectively. The difference between the tube voltage and the cathode fall gives the voltage V across the positive column. The electric field of the positive column is then V/l where l is the length of the column. l will be taken to be the length between the anode and cathode. Hence,

$$E_{max} = \frac{1100V}{30\ cm} = 36.7\ Vcm^{-1} \qquad (3.4)$$

$$E_{min} = \frac{1050V}{30\ cm} = 35\ Vcm^{-1} \qquad (3.5)$$

As a first approximation, the gas density will be taken to be the density without a discharge. At a pressure

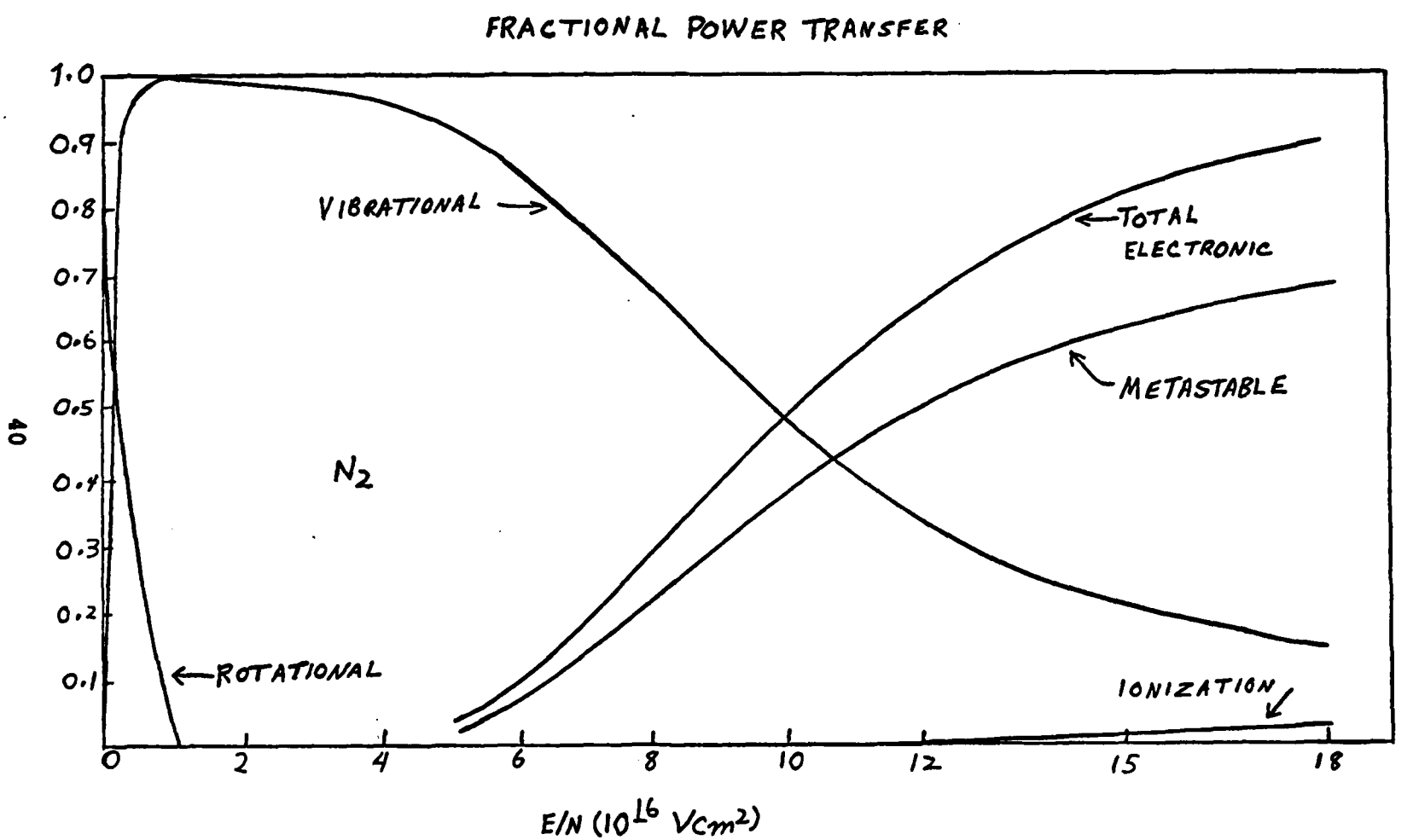

Figure 9. Fractional Power Transfer in a N_2 Discharge (Ref 3)

of 2 torr and a temperature of 293°K, the density of n=2.505 X 10^{19} $(\frac{2}{760})$ = 6.59 X 10^{16} cm^{-3} (see Appendix B). Using this value for n and equations (3.4) and (3.5), the maximum and minimum E/n values are given respectively by

$$E_{max}/n = 5.57 \times 10^{-16} \text{ Vcm}^2 \qquad (3.6)$$

$$E_{min}/n = 5.31 \times 10^{-16} \text{ Vcm}^2 \qquad (3.7)$$

At these two values of E/n, over 90% of the power goes into vibrational excitation of which some smaller fraction goes eventually into translational energy. For an E/n of 18 x 10^{-16} Vcm^2, ionization accounts for only 5 % of the power input. The rest of the power is transferred to the excitation of the metastable state and total electronic excitation.

40% CO_2/50% N_2/10% Ar

The chemistry of a CO_2/N_2/Ar discharge is illustrated in Fig. 10. The initial CO_2 concentration of 40%, dropped to 30% at a discharge current of 10 mA. The maximum dissociation occurred at a current of 80 mA when the concentration reached approximately 15%. The saturation point also appeared to occur around 80 mA. The fractional dissociation was 62.5% compared to 44% in CO_2/Ar discharge. Although a greater number of molecules were dissociated in a CO_2/Ar discharge, the fraction of CO_2 dissociated was greater in the CO_2/N_2/Ar mixture. In addition to CO_2 dissociation by the mechanism illustrated in (3.1) and (3.2), there is

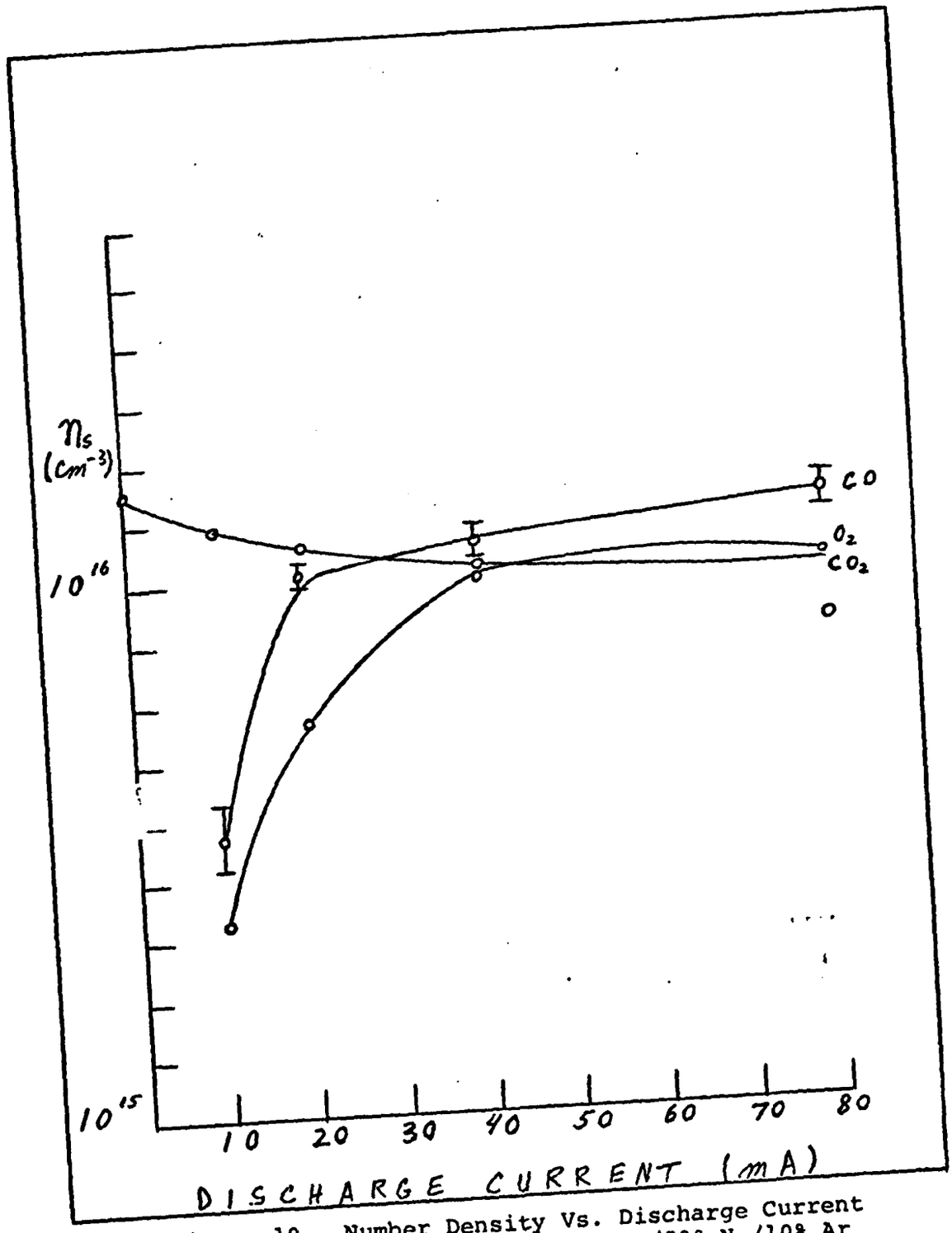

Figure 10. Number Density Vs. Discharge Current of the Major Species in a 40% CO_2/50% N_2/10% Ar Discharge (Experimental)

possible dissociation by the collision of excited N_2 molecules. This explains the greater fraction of CO_2 molecules dissociated in the mixture. However, CO_2 dissociation by excited N_2 molecules is a hypothesis which requires rigorous testing.

In a mixture of 33% CO_2 and 67% N_2, Smith and Austin (Ref 20:315) reported a CO_2 dissociation of 20% above a CO_2 partial pressure of 1.2 torr and at a discharge current of 60 mA. The partial pressure of CO_2 in the $CO_2/N_2/Ar$ mixture used in this experiment was

$$p_s = \frac{H_s}{H} p$$

$$p_s = (4.648/11.62)(2) = 0.8 \text{ torr} \qquad (3.8)$$

where H_s is the flow rate of CO_2, H is the total flow rate of the mixture, and p is the total pressure of the mixture (see Appendix B). At 60 mA, the fractional dissociation was 60%. This is higher than Smith and Austin's value of 25%. No exact comparison can be made since Smith and Austin gave no mention of gas residence time.

The concentration of CO molecules rose as much as 8.5% at a discharge current of 10 mA and 33% at 80 mA. As in the case for CO_2/Ar, there was no indication of CO dissociation at high discharge currents. This observation was confirmed when no rise in the C signal occurred. The CO percentage in the range from 10 - 40 mA is slightly higher than that shown in Fig. 10. The reason is that CO and H_2 have approximately the same mass number; and in determining

the CO signal, a constant N_2 signal was subtracted from the total signal at mass number 28. But there was 1% N_2 dissociation, and there is no apparent reason why N_2 should dissociate in a mixture containing CO_2 but not in a N_2/Ar discharge. This same behavior was noticed in the CO_2/N_2/He/Ar discharge except that the N concentration began to increase slightly past 40 mA.

With this small amount of N_2 dissociation, various nitrogen oxides should be detectable. N_2O could not be detected because it has the same or nearly the same mass number as CO_2, and the resolution of the quadrupole is not sufficient in resolving the N_2O and CO_2 signals. Thus, N_2O may have been formed. NO_2 was not formed in detectable quantities. This conclusion was based on the fact that a signal appeared at mass number 46 with no discharge. The signal was attributed to $C^{14}O_2$. If NO_2 was formed, then its signal would increase the $C^{14}O_2$ signal. However, this was not the case. There was a trace amount of NO, and great care was taken in identifying it. In a CO_2/Ar discharge, a signal at mass number 30 appeared only at high discharge currents. Since there was a little water contamination (<1%), this species was tentatively identified as CH_2O. It is safe to assume that CH_2O appeared at high discharge currents in the CO_2/N_2/Ar mixture so that its signal was added to the NO signal. At low currents, the signal at mass number 30 appeared; and it was attributed to NO. The concentration of NO stayed at a constant 0.29% of the total

ion current from the spectrometer in the range of 10 - 80 mA. NO was not detected in a N_2/Ar discharge since there was no detectable N_2 dissociation.

The O_2 concentration rose from 5% at 10 mA to 16.5% at 60 mA. Past 60 mA, the concentration appeared to decrease; however, more data points are required to reach a definite conclusion. If the O_2 concentration indeed decreased, then the decrease was at a much slower rate than that shown in Fig. 8. As can be seen in Fig. 8, the O_2 concentration decreased rapidly as the discharge current was increased past 50 mA in a CO_2/Ar discharge. There are two possible mechanisms for the slower decrease in a CO_2/N_2/Ar discharge. One is that the reaction rate of O_2 formation on the walls of the discharge tube increased (i.e., the diffusion of O to the walls increased), and the other is that less dissociation occurred through electron impact.

10% CO_2/80% He/10% Ar

Fig. 11 shows the discharge chemistry of a CO_2/He/Ar mixture. The purpose of the He in CO_2 lasers is to relax the lower laser level of the CO_2 molecule to the ground state. Thus, the He is not expected to influence the chemistry of the discharge much (except in the case of three body reactions involving He). The saturation point of CO_2 dissociation was approximately 2.5% concentration at a discharge current of 90 mA. This point was determined by extrapolating the curve in Fig. 11 to high values of the

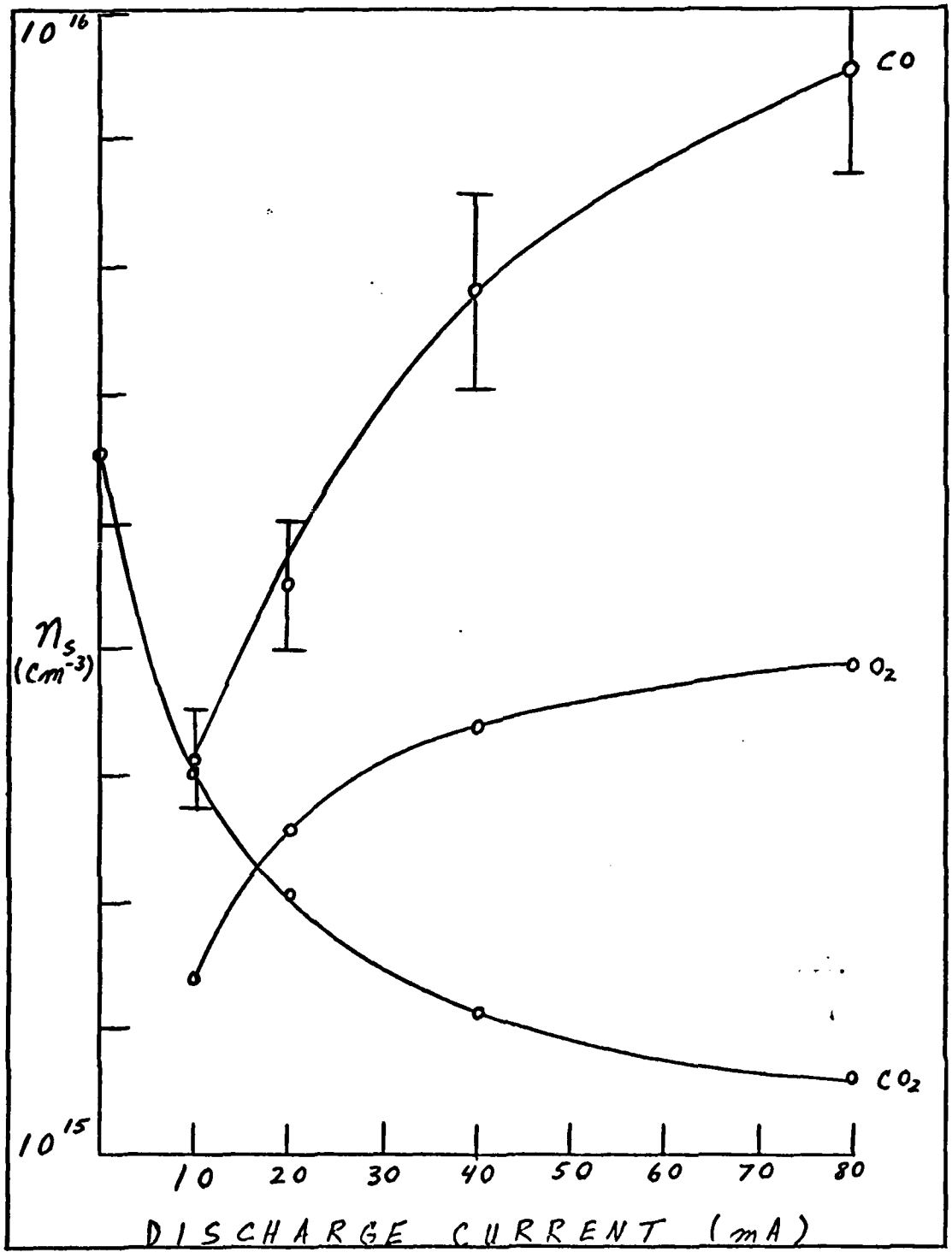

Figure 11. Number Density Vs. Discharge Current of the Major Species in a 10% CO_2/80% He/10% Ar Discharge (Experimental)

current. The fractional dissociation was 74%, and it was higher than the dissociation in CO_2/Ar and CO_2/N_2/Ar. At 40 mA, the dissociation was 65% which is high compared to the Gasilevich et al. value of 60% dissociation (Ref 11:88). They had similar experimental conditions except that the ratio of the CO_2 concentration to the He was 1:9, and the diameter of the tube was 22 mm compared to a diameter of 25 mm in this experiment. They also reported that the dissociation depended on the diameter of the tube so that this may account for the difference between their values of the dissociation and the value obtained in this experiment. If CO_2 dissociation occurs through mechanisms (3.1) and (3.2), it is difficult to explain why a greater fraction of CO_2 molecules are dissociated. Since He relaxes the vibrational excitation of CO_2, there should be more CO_2 molecules in the ground state. However, since He has a high ionization potential ($\simeq$ 24V) the electrons are expected to be more energetic in a predominantly He discharge, thereby causing more dissociations.

The measured percentage of CO in the discharge was higher than the original CO_2 concentration between 35 and 80 mA as shown in Fig. 11. At 10 mA, the concentration of CO reached 6.5% of the original number density; however, at a discharge current of 80 mA, the concentration was 14%. This can be explained by noting that the spectrometer function shows a large dispersion at mass 28, and the same spectrometer factor for CO was used in the data reduction

of all the mixtures considered in this experiment. Although the percentages of CO in Fig. 11 may be a little high, the basic shape of the curve is still correct. There was no problem with the O_2 concentration being higher than the original CO_2 concentration. The O_2 concentration also showed no decrease with increasing discharge current.

8% CO_2/ 11% N_2/ 71% He/ 10% Ar

The fractional dissociation of CO_2 in a $CO_2/N_2/He/Ar$ discharge was up to 76% as shown in Fig. 12. The dissociation was higher than any previous mixture considered. An important trend was noted: as the original CO_2 concentration in a mixture was decreased, greater dissociation of CO_2 occurred. The partial pressure of CO_2 was 0.16 torr, and the dissociation at 60 mA was 72.5%. Smith and Austin reported a dissociation of 68% for the same conditions of CO_2 partial pressure and discharge current (Ref 20:315). No satisfactory comparison between the dissociation reported here and that reported by Smith and Austin can be made since they did not state their gas residence times, as mentioned earlier.

One underlying mechanism that may explain the dependence of CO_2 dissociation on CO_2 concentration and mixture is CO and O recombination at the walls of the discharge tube. This recombination at the walls has already been introduced as one of the reasons why atomic oxygen was undetectable. Some of the parameters that radial diffusion

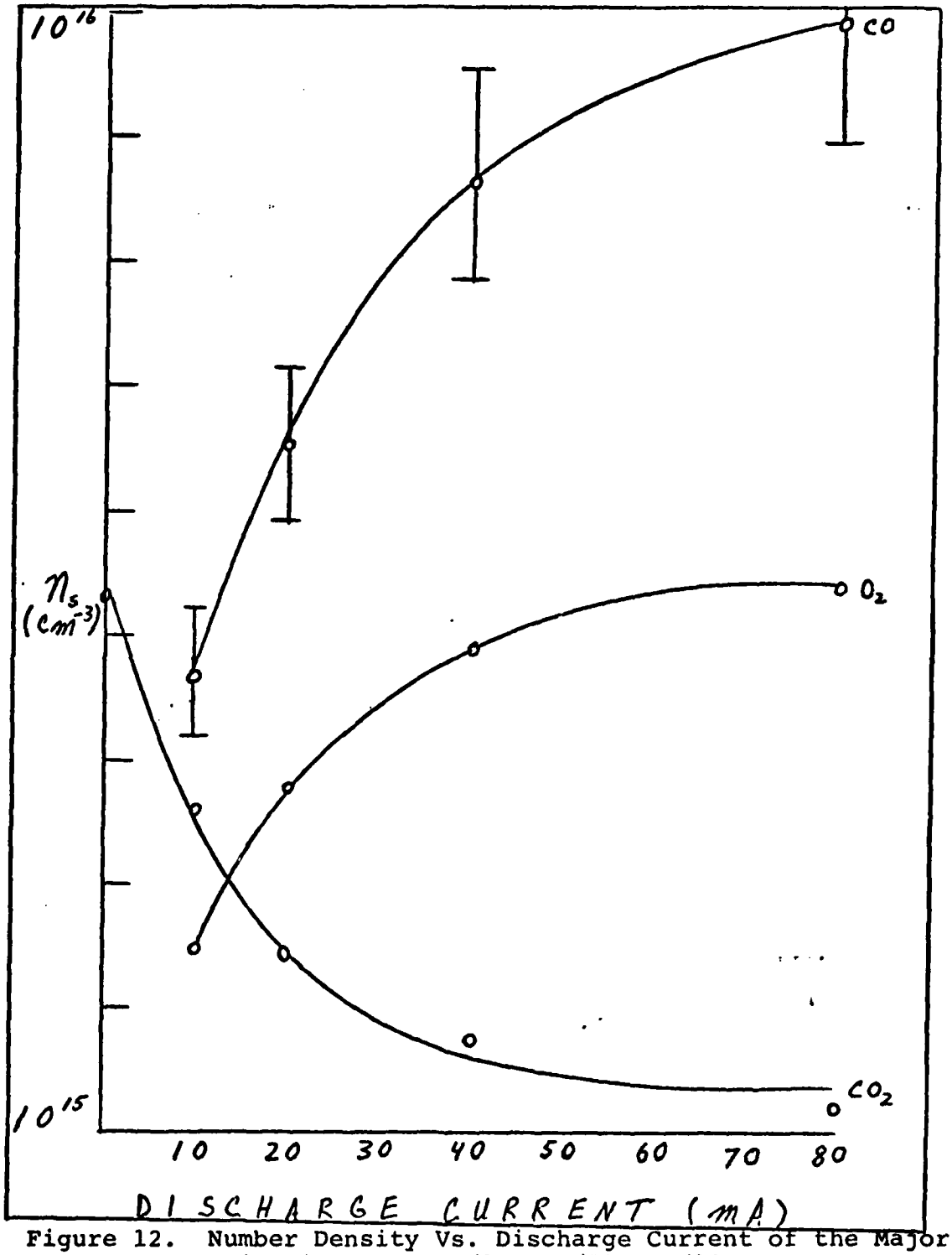

Figure 12. Number Density Vs. Discharge Current of the Major Species in a 8% CO_2/11% N_2/71% He/10% Ar Discharge (Experimental)

depends on are the gas mixture, the partial pressure of the molecular species in question, the total gas pressure; and the temperature. By knowing the rate of CO and O diffusion to the walls and the probability of CO and O encounters at the walls, a reaction rate constant can be computed. Recombination at the walls also depends on tube geometry and gas flow. This is a possible explanation as to why Gasilevich et al. found that CO_2 dissociation depended on the tube geometry and gas flow (Ref 11).

In Fig. 12, the CO concentration exceeds the initial CO concentration at a discharge current of 15 mA. As noted earlier, this discrepancy can be attributed in part to an inaccurate spectrometer factor for CO in this particular mixture. There was no indication of saturation of the CO percentage at high currents. However, small amounts of carbon were detected. The percentage of C in the spectrometer ion current fluctuated from 0.26% at 10 mA to 0.087% at 80 mA. The C may have come from CO dissociation at high currents; however, this is not apparent from Fig. 12. The dissociation of O_2 at high currents was also not detected as evident from Fig. 12. The O_2 concentration saturated at 8% of the original number density which was the initial CO_2 concentration. The high saturated concentrations of CO and O_2 apparently are due in part to the inaccuracy of their respective spectrometer factor.

As in the $CO_2/N_2/Ar$ mix, there was a small amount of N_2 dissociation. The N concentration fluctuated over

the whole range of discharge currents similarly to the C concentration mentioned in the previous paragraph. For this reason, there must have been a fluctuation in the electronics or total gas flow. With this small amount of N_2 dissociation, there was again a strong possibility of nitrogen oxides in the discharge. There was no trace of NO_2, and the presence of N_2O could not be detected because of its similarity in mass number with that of CO_2. As stated in the case of a $CO_2/N_2/Ar$ discharge, the spectrometer cannot discriminate between N_2O and CO_2 because of its limited resolution. The NO stayed at a constant 0.5% in the range of 10-80 mA. This percentage was greater than the 0.2% reported in the case of a $CO_2/N_2/Ar$ discharge. Thus, the formation of NO was greater in a $CO_2/N_2/He/Ar$ discharge than in a $CO_2/N_2/Ar$ discharge.

A signal at mass number 29 was observed, and it was partly attributed to the formation of CHO. This CHO is extremely plausible since traces of free carbon and atomic hydrogen were detected. The presence of atomic hydrogen will be explained in the next section. The signal at mass number 29 was also observed in the case of a pure N_2 discharge and was tentatively identified as $N^{14}N^{15}$. Therefore, the signals of CHO and $N^{14}N^{15}$ may very well be combined in the $CO_2/N_2/He/Ar$ mixture.

The Influence of Water Contamination

In all of the mixtures considered, there was less than one percent water contamination. The following

additional species were detected in all mixtures at low discharge currents: H_2O, OH, and H_2. At high currents, the following were detected: H_2O, OH, and H. The reason that atomic hydrogen appeared at high currents was that at these higher currents, dissociation of H_2 occurred. If water was not present, then CHO and CH_2O in addition to the species mentioned above would not have appeared.

IV. Theoretical Prediction of Plasma Chemistry Processes

In the following theoretical treatment, it will be assumed that the gas pressure is low enough so that certain ternary reactions are negligible. This assumption is justified because the gas pressure used in this experiment was 2 torr, and ternary reactions at this pressure do not contribute much to the chemistry. Only those with sizeable rates will be considered. However, the bulk of the reactions considered in this analytical model will be binary.

Binary Reactions

Consider the binary reaction m involving species A_i and A_j in which species A_k and A_l are formed:

$$A_i + A_j \underset{k_r}{\overset{k_f}{\rightleftharpoons}} A_k + A_l \tag{4.1}$$

k_f and k_r are the forward and reverse reaction rates respectively. The populating or depopulating rate of A_k is given by

$$\left(\frac{d[A_k]}{dt}\right)_m = k_f[A_i][A_j] - k_r[A_k][A_l] \tag{4.2}$$

where the brackets denote number density. $\left(\frac{d[A_l]}{dt}\right)_m$, $-\left(\frac{d[A_i]}{dt}\right)_m$, and $-\left(\frac{d[A_j]}{dt}\right)_m$ are also equal to the expression on the right hand side of equation (4.2). Equation (4.2)

can be generalized to include the case where more than two species are formed from the reaction of A_i with A_j.

It will be assumed that the formation and depletion of a particular atomic or molecular species are due entirely to chemical reactions. Under this assumption, the total rate equation for species A_k is

$$\frac{d[A_k]}{dt} = \sum_m \left(\frac{d[A_k]}{dt}\right)_m \tag{4.3}$$

where the sum is over all reactions that form A_k. The result of this formulation is a set of coupled nonlinear differential equations involving the number densities of the molecular species in the laser discharge. A closed analytical solution of these equations is not feasible. Therefore, they are solved numerically.

The treatment presented here on binary reactions can easily be extended to include ternary reactions. The only difference is that since three species are reacting, the first term on the right hand side of equation (4.2) includes the product of the three number densities.

Chemistry Code

A list of the important reactions and their respective rate constants are given in Appendix C. These were not the only ones considered, but they are the ones that influenced the chemistry the most. A few of the reactions have a temperature and average electron energy dependence. The

temperature was taken to be 300°K, and the average electron energy was taken to be 1 eV. Ion reactions were not considered because it was assumed that the neutral chemistry was perturbed little by them. Also, the reverse rate constants of the reactions in Appendix C were set equal to zero because they were not available. The resultant differential equations were solved by the modified Euler method. The reactions, their rates, and the differential equation solver comprise the code which was developed by M. Stamm (Ref 21).

The code required a value for the electron number density, and this value was kept constant throughout the temporal evolution of the species. To find this value, an approximate E/n for the mixture was calculated using the same method as that outlined in the case for pure N_2. Next, for the value of E/n computed, the drift velocity of the electrons was determined. Finally, the number density of electrons was found from the following relation:

$$n_e = \frac{I}{qv_dA} \qquad (4.4)$$

where I is the measured discharge current, A is the cross-sectional area of the discharge tube, q is the magnitude of the electronic charge, and v_d is the drift velocity of the electrons. The drift velocity was taken from the curves in Appendix D.

In each mixture, four values of the reduced field were computed corresponding to four values of the discharge

current (10, 20, 40, and 80 mA). Consequently, this gave four values of the electron number density. The code was run for each value of n_e, and the species concentrations after a time of 1 sec were compared to the experimental values. The 1 sec was consistent with the experimental value of the gas residence time.

It was found that the published value of the rate constant (e.g., Ref 19) for CO_2 dissociation by electron impact did not result in CO_2 dissociation in agreement with experiment. When the published value was used in the code, the CO_2 concentration went essentially to zero in 1 sec. The dissociation was far greater than that experimentally observed. A rate constant providing agreement with the experiment was obtained in the following way. In the CO_2 derivative, the term involving CO_2 dissociation by electron impact is much greater than any other term in the same rate equation. Hence, the CO_2 rate equation can be given approximately by

$$\frac{d[CO_2]}{dt} = - k_f[CO_2]n_e \qquad (4.5)$$

Integrating (4.5) and applying the initial condition that at t=0, $[CO_2] = [CO_2]_o$, the following result is obtained:

$$[CO_2] = [CO_2]_o \, e^{-k_f n_e t} \qquad (4.6)$$

At t=1 sec,

$$[CO_2] = [CO_2]_o \, e^{-k_f n_e} \qquad (4.7)$$

Solving for the forward rate constant k_f, the following is obtained:

$$k_f = \frac{1}{n_e} \ln \left(\frac{[CO_2]_o}{[CO_2]} \right) \qquad (4.8)$$

$[CO_2]_o$ and $[CO_2]$ can be obtained from experiment so that an effective rate constant for a given n_e suitable to the experiment can be determined. When the rate, calculated from (4.8), is used in the code, then the theoretical curve for the CO_2 concentration vs. discharge current approximates the experimental curve.

Theoretical and Experimental Comparison

As evident from Figs. 8 and 10-16, there is good agreement between the experimental and theoretical CO_2 concentration. As mentioned earlier, this agreement is due to the fact that the rate constant was computed from the experimentally observed dissociation assuming a single exponential decay and a constant electron number density. The small difference between the two curves is due to the fact that the other terms in the CO_2 derivative were neglected. The corresponding rise in CO shows fair agreement between theory and experiment in all of the mixtures. It should be remembered that a possible source of error in the experimental measurement of CO is the inaccuracy of the spectrometer factor used in normalizing the experimental CO percentage. The calculated rate constant indicates that CO_2 dissociates by the following mechanism:

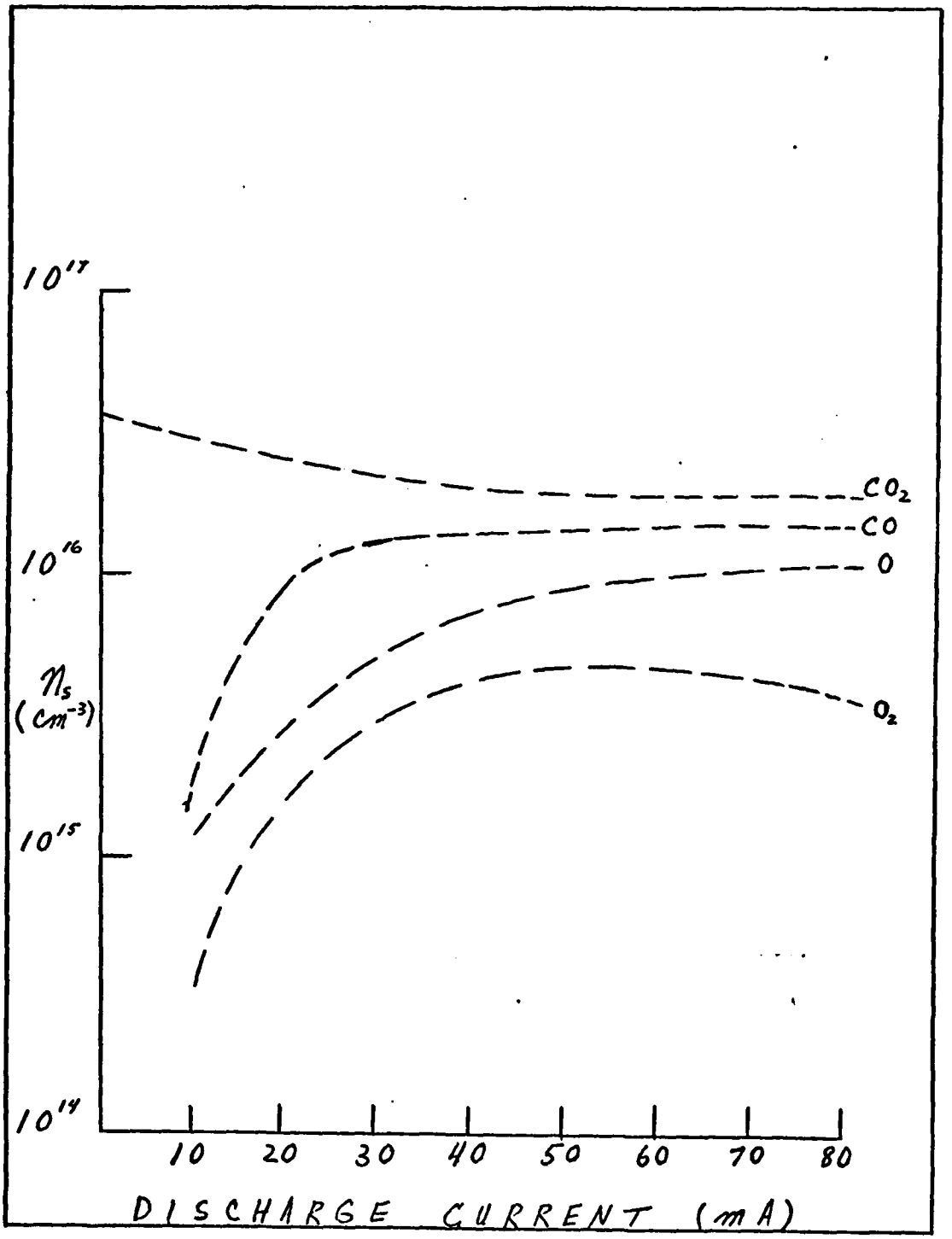

Figure 13. Number Density Vs. Discharge Current of the Major Species in a 90% CO_2/10% Ar Discharge (Theoretical)

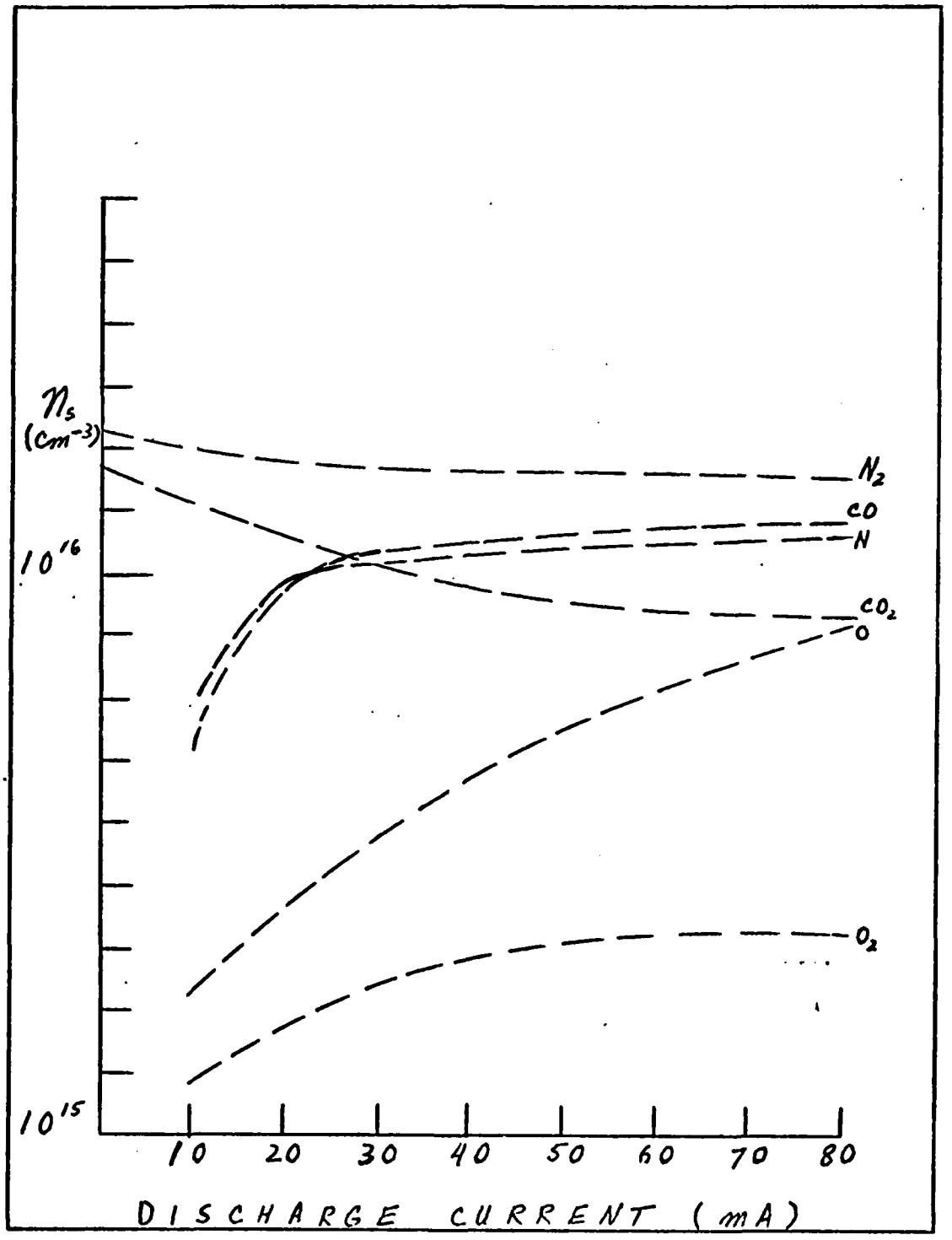

Figure 14. Number Density Vs. Discharge Current of the Major Species in a 40% CO_2/50% N_2/10% Ar Discharge (Theoretical)

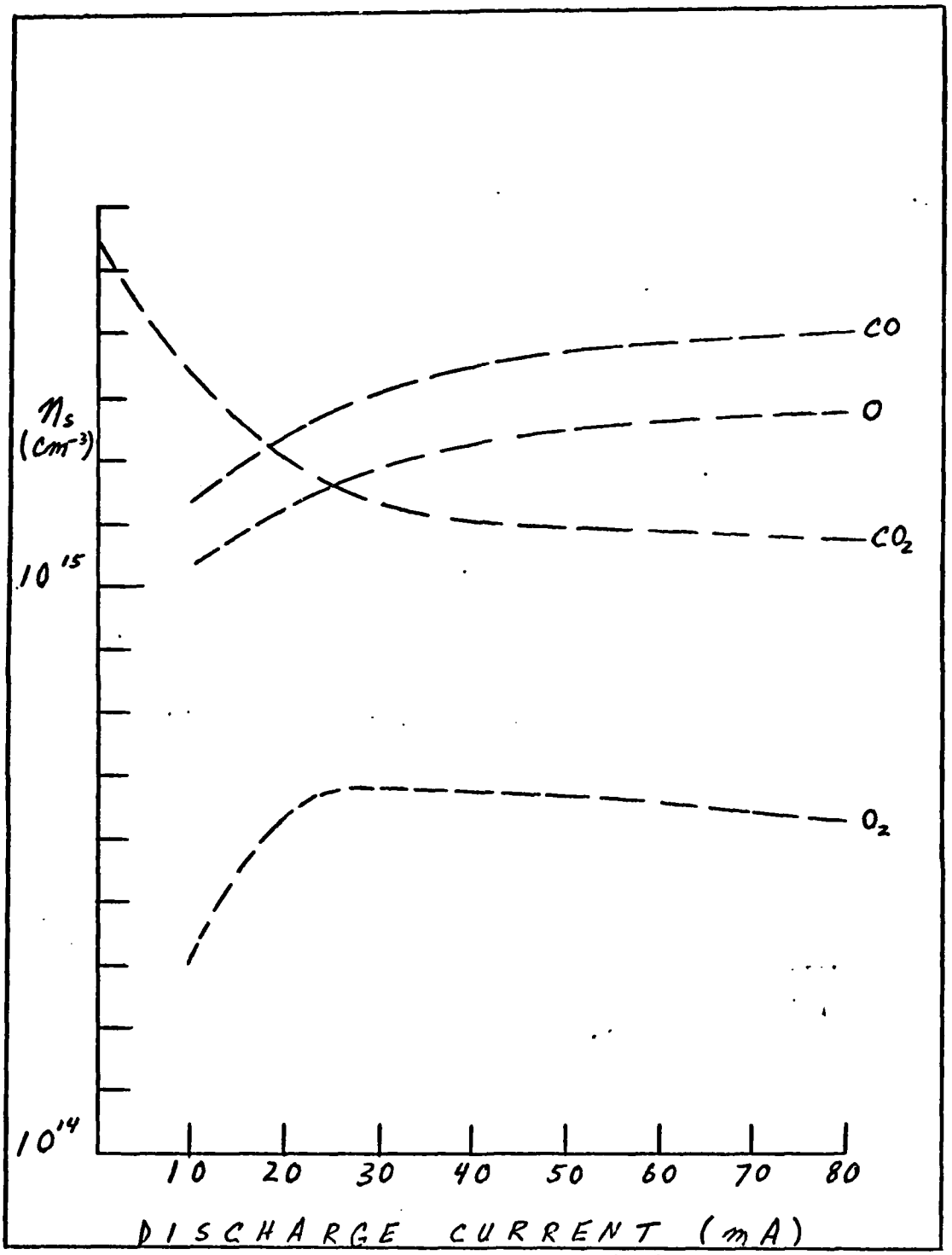

Figure 15. Number Density Vs. Discharge Current of the Major Species in a 10% CO_2/80% He/10% Ar Discharge (Theoretical)

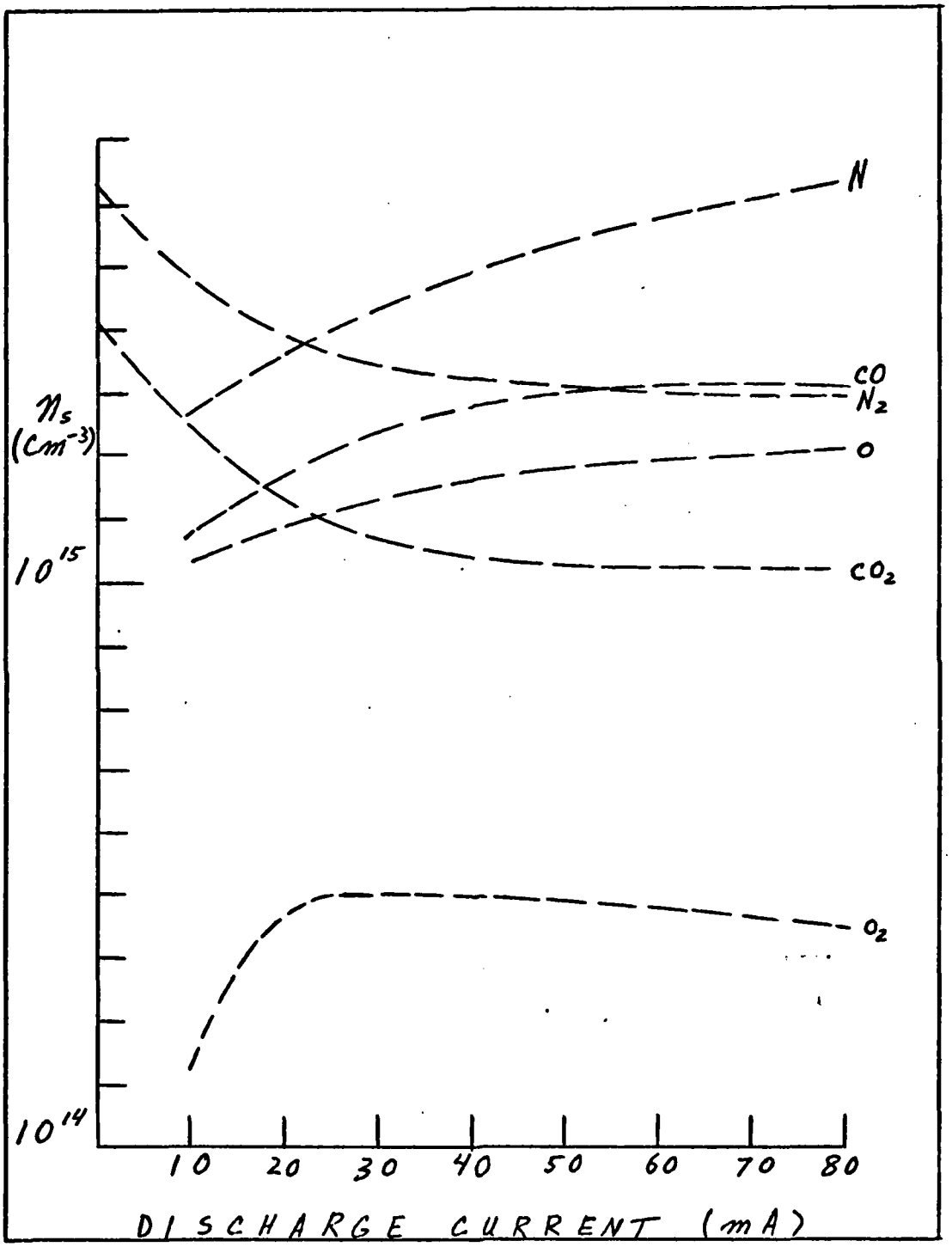

Figure 16. Number Density Vs. Discharge Current of the Major Species in a 8% CO_2/11% N_2/71% He/10% Ar Discharge (Theoretical)

$$CO_2 + e^- \rightarrow CO + O + e^- \qquad (4.9)$$

As indicated in Appendix C, the rate constant calculated from equation (4.8) depends on the mixture and is lower than the published value.

The model predicts that the concentration of O exceeds O_2 in all mixtures. In CO_2/Ar and CO_2/He/Ar, the O_2 is lost by

$$O_2 + e^- \rightarrow O + O + e^- \qquad (4.10)$$

with a rate constant of 1×10^{-9} cm^3 s^{-1} (Ref 19). This rate is larger than the recombination rate of atomic oxygen given by

$$O + O + M \rightarrow O_2 + M \qquad (4.11)$$

where the rate constant is 7.2×10^{-33} cm^6 s^{-1} (Ref 6), and M stands for all species in the discharge and the wall. In addition to reaction (4.10), atomic oxygen is formed by

$$N + O_2 \rightarrow NO + O \qquad (4.12)$$

and

$$N + NO \rightarrow N_2 + O \qquad (4.13)$$

in the mixtures containing nitrogen. The rate constants for (4.12) and (4.13) are given by 8.5×10^{-17} cm^3 s^{-1} (Ref 6) and 2.7×10^{-11} cm^3 s^{-1} (Ref 6) respectively. The reason that reactions (4.12) and (4.13) are important is due to the large amount of nitrogen dissociation. In a

current range of 10 - 18 mA, the N percentage rises from 11 to 25% in $CO_2/N_2/Ar$ and 5 to 11% in $CO_2/N_2/He/Ar$. The rate constant for N_2 dissociation by electron impact had to be assumed (1×10^{-9} cm^3 s^{-1}), and it may have been too high because the high N concentrations were not observed experimentally.

The dominant nitrogen oxide in both $CO_2/N_2/Ar$ and $CO_2/N_2/He/Ar$ is NO as observed experimentally (<1%). It is formed by reaction (4.12) and by

$$N + O + M \rightarrow NO + M \qquad (4.14)$$

where the rate constant is 1×10^{-32} cm^6 s^{-1} (Ref 6). In spite of the low rate constant of reaction (4.14), the importance lies in the large concentration of N and O. The additional reaction given by

$$O + NO_2 \rightarrow O_2 + NO \qquad (4.15)$$

which has a rate constant of 9.2×10^{-12} cm^3 s^{-1} (Ref 6) is important in $CO_2/N_2/Ar$. Since reaction (4.15) has a fast rate, NO_2 does not build up in quantities comparable to NO. This is confirmed by the model.

V. Conclusions and Recommendations

CO_2 dissociation appears to depend on initial CO_2 concentration and mixture. Dissociation is smaller with greater amounts of initial CO_2 and vice versa. One method to use in finding out whether dissociation depends on mixture is to vary the initial concentration of CO_2 within one mixture. The ultimate reason for this behavior may lie in the kinetics of the discharge.

The calculated rate constant for CO_2 dissociation lies between those of dissociative attachment and dissociation by electron impact (Ref 19). This calculated rate is larger than that of dissociative attachment by a factor of 10^3. Therefore, it is concluded that CO_2 dissociation occurs by electron impact. The difference between the published rate and the calculated one can be attributed to experimental error and chemistry changes in the flow from orifice to detector. These chemistry changes undoubtedly change the concentrations of all reactant species. The problem of chemistry changes in a molecular beam can be avoided by direct spectroscopic measurements of the source in determining the concentration of a particular species.

The concentration of atomic oxygen exceeds that of molecular oxygen in all mixtures. The reason is due to the fact that the dissociation rate of O_2 by electron impact

is larger than the recombination rate of 0 to form O_2. This conclusion comes from the model which did not include wall recombination. Experimentally, molecular oxygen was detected in higher concentrations than that predicted by the model with no traces of atomic oxygen observed. The O_2 concentration reaches a maximum between discharge currents of 40 and 60 mA, and then it starts to decrease with increasing current. This behavior of the O_2 concentration, predicted by the model, occurs in all mixtures except $CO_2/N_2/Ar$. Experimentally, the behavior of the O_2 concentration mentioned above occurred only in the CO_2/Ar discharge.

Little N_2 dissociation occurs in a pure N_2 discharge. Most of the input power goes into vibrational excitation of which a smaller portion goes eventually into translational energy. However, the dissociation of N_2 increases when it is added to mixtures containing CO_2. This dissociation is less than 1%, and the rate constant is somewhat less than the assumed value (1×10^{-9} cm^3 s^{-1}). A possible explanation is that in a mixture containing CO_2 and N_2, N_2 dissociation occurs by the collision of an excited CO_2 molecule with a N_2 molecule.

The dominant nitrogen oxide in a $CO_2/N_2/Ar$ or $CO_2/N_2/He/Ar$ discharge is NO. In both cases, this was observed experimentally and is also predicted by the chemistry code. The NO concentration never exceeds 1% in the discharge current range of 10 to 80 mA. The concentrations of NO_2 and N_2O are essentially zero in this current range.

If there is less than 1% water contamination, H_2O, OH, and H_2 appears in all mixtures at low currents. Atomic hydrogen is present at higher currents due to the dissociation of H_2. In the mixtures containing CO_2, the additional species CHO and CH_2O are present. The species CHO and CH_2O can be identified positively if the gas is first dried before entering the discharge region.

The kinetic modeling can be improved in two important ways. First, a calculation of the electron energy distribution using a solution to the Boltzmann energy equation for the E/n and mixture of gases to which it pertains should be made. Then, an integration of this distribution with the appropriate inelastic electron scattering cross-sections could give the proper electron kinetic rates. Secondly, the model should be extended to include non-neutral chemistry so that ionization and recombination are properly treated. Such a model will provide more accurate information on the plasma chemistry occurring in CO_2 laser discharges.

Bibliography

1. Alger, S. R. and J. A. Rees. "Positive and Negative Ion Reactions in Carbon Dioxide," J. Phys.D: Appl. Phys., 10: 957-968 (1977).

2. Austin, J. M. and A. L. S. Smith. "Analysis of Positive Ions in CO_2 Gas Laser Systems," J. Phys. D: Appl. Phys., 5: 468-475 (1972).

3. Bailey, William. Collision Induced Dissociation of Diatomic Molecules. Ph.D. thesis. Wright-Patterson AFB, Ohio: Air Force Institute of Technology, June 1978.

4. Bletzinger, Peter et al. "Influence of Contaminants on the CO_2 Electric-Discharge Laser," IEEE Journal of Quantum Electronics, QE-11: 317-323 (July 1975).

5. Buser, R. G. and J. J. Sullivan. "Initial Processes in CO_2 Glow Discharges," Journal of Applied Physics, 41: 472-479 (February 1970).

6. Cason, Charles et al. A Small Scale Closed Cycle Circulator Experimental Plan For Repetitively Pulsed 200K High Pressure Electric Discharge Lasers. Technical Report RH-76-12. Redstone Arsenal, Al.: U.S. Army Missile Command, 2 August 1976.

7. Corvin, Kutszegi K. and S. J. B. Corrigan. "Dissociation of Carbon Dioxide in the Positive Column of a Glow Discharge," The Journal of Chemical Physics, 50: 2570-2574 (March 1969).

8. Coxon, P. and J. L. Moruzzi. "Ion-Molecule Reactions in CO_2 and CO_2-CO Mixtures," J. Phys. D: Appl. Phys., 10: 967-977 (1977).

9. Elliot, C. J. et al. Electron Transport Coefficients and Vibrational Excitation Rates for Electrically Excited CO_2 Gas Lasers. Informal Report LA-5572-MS. Los Alamos, N.M.: Los Alamos Scientific Laboratory, April 1974.

10. Fite, Wade L. Expansion of Gases from Molecular Beam Sources. Research Note #1. Pittsburgh, Penn.: Extranuclear Laboratoriies, Inc., January 1971.

11. Gasilevich, E. S. et al. "Carbon Dioxide Dissociation in a CO_2 Laser," Soviet Physics-Technical Physics, 14: 86-91 (July 1969).

12. Karube, Norio and Eiso Yamaka. "Mass-Spectrometric Studies of a Sealed CO_2 Laser," Journal of Applied Physics, 41: 2031-2042 (April 1970).

13. Pace, Paul W. and Marc Lacombe. "A Sealed High-Retetition-Rate TEA CO2 Laser," IEE Journal of Quantum Electronics, QE-14: 263-274 (April 1978).

14. Paul, W. et al. "Das elektrische Massenfilter als Massenspektrometer und Isotopentrenner," Zeitschrift fur Physik, 151: 143-182 (April 1958).

15. Prince, J. F. and A. Garscadden. "Negative Ion Species in CO_2-N_2-He Discharges," Applied Physics Letters, 27: 13-15 (July 1975).

16. Research Note #4. Electric Quadrupole Mass Filters. Pittsburgh, Penn.: Extranuclear Laboratories, Inc., (undated).

17. Sherman, Frederick S. "Hydrodynamical Theory of Diffusive Separation of Mixtures in a Free Jet," The Physics of Fluids, 8: 773-779 (May 1965).

18. Shields, H. and A. L. S. Smith. "Negative Ion Effects in CO_2 Convection Laser Discharges," Appl. Phys., 16: 111-118 (1978).

19. Shields, H. et al. "Negative Ion Effects in TEA CO_2 Lasers," J. Phys. D: Appl. Phys., 9: 1587-1603 (1976).

20. Smith, A. L. S. and J. M. Austin. "Dissociation Mechanism in Pulsed and Continuous CO_2 Lasers," J. Phys. D: Appl. Phys., 1: 314-322 (1974).

21. Stamm, Michael (private communication).

22. Thoenes, Jurgen and S. C. Kurzius. Plasma Chemistry Processes in Pulsed Electric Discharge Lasers. Technical Report RH-CR-76-12. Redstone Arsenal, Al.: U.S. Army Missile Command, August 1976.

23. von Engel, A. Ionized Gases (Second Edition). London: Oxford University Press, 1965.

24. Wiegand, W. J. and W. L. Nighan. "Plasma Chemistry of CO_2-N_2-He Discharges," Applied Physics Letters, 22: 583-586 (January 1973).

Appendix A

Data Reduction

When determining the true percentage of each gas component in a mixture, three factors must be considered. These factors are the spectrometer characteristics, the density change due to the rise in gas temperature under discharge conditions, and the ionization cross section. The spectrometer function incorporates the spectrometer characteristics, and it is discussed in the experimental arrangement and procedure section. The remaining two factors will be discussed below.

Argon Correction Factor

The number density of the source changes under discharge conditions due to gas heating. Since Ar does not influence the chemistry of the source, it can be added in small percentages to monitor this change. Ar may contribute to third body reactions, but the pressure of the source is low enough such that the probability of third body reactions is very small. The Ar correction factor is defined by:

$$K_{Ar} \equiv (PH)_{Ar}/PH'_{Ar} \qquad (A.1)$$

where $(PH)_{Ar}$ is the "peak height" in cm deflected by the chart recorder of the Ar signal in the cold gas (no

discharge), and $(PH)'_{Ar}$ is that same "peak height" in the discharge. Experiments have shown that in general, $K_{Ar}>1$. The reason being that the number density decreases under discharge conditions. However, there have been occasions when K_{Ar} was less than or equal to one. The reason is thought to be due to a fluctuation in gas flow or to the electronics. All of the peak heights in the discharge are corrected for by K_{Ar}.

Ionization Cross Section

From equation (2.16), it can be seen that the ionization cross section of each molecular species in the source must be known. This total cross section corresponds to the particular energy setting of the ionizer. It is desirable to have the ionizer energy 2-3 eV above the greatest ionization energy expected among the molecular species in a mixture. This setting of the ionizer energy reduces the possibility of double ionization and molecular dissociation occurring in the ionizer. In this experiment, the highest ionization energy is that of He (24.58 eV). A typical setting of the ionizer energy would then be 27.0 eV. When the contact potential is taken into account, the meter reading is 27.0 eV plus the contact potential. The contact potential is explained in the experiment arrangement and procedure section. It is found experimentally that the best signal results are achieved with an energy between 65 and 70 eV.

The Reduction Process

If the ionization cross section for an additional species is known and the signal is measured, equation (2.16) can be solved for n_s giving the total number density of species s that is produced in the discharge:

$$n_s = \frac{(PH)_s}{\sigma_s F_s} \qquad (A.2)$$

When the argon correction factor is included, the reduced percentage of molecular species s becomes:

$$n_s = \frac{(PH)_s K_{Ar}}{\sigma_s F_s} \qquad (A.3)$$

Appendix B

Residence Time and Number Density Calculation

Consider the discharge tube presented as G in Fig. 1. Assuming Poiseuille flow through this tube, the radial velocity profile is parabolic. As a result, the gas near the walls have a slower velocity and thus stay in the discharge longer. It is the gas near the walls that the spectrometer samples because the sampling orifice is located at the wall. In the following discussion, it is assumed that all the molecules travel through the tube at the same rate.

The volume of gas that passes a specified point in time t is given by:

$$V = vtA \qquad (B.1)$$

where v is the velocity of the flow, and A is the cross sectional area of tube (which is assumed constant). Solving for the flow velocity in equation (B.1), the following result is obtained:

$$V = \frac{V}{ta} \qquad (B.2)$$

$\frac{V}{t}$ is the volume flow rate past a point within the tube. This flow rate is usually given in standard cubic centimeters per minute (SCCM). It is the volume occupied by a given gas at standard temperature and pressure (STP).

Standard temperature and pressure are defined as 20°C and 760 mm of Hg (torr) respectively. Assuming an ideal gas, the number density of molecules in one standard cubic centimeter is given by:

$$n_o = \frac{P_o}{kT_o}$$

$$n_o = 2.505 \times 10^{19} \text{ cm}^{-3} \qquad \text{(B.3)}$$

where P_o and T_o are the standard values of pressure and temperature respectively, and k is Boltzmann's constant.

If the temperature is constant, then the volume occupied at any arbitrary pressure P is given by

$$V = \frac{P_o}{P} V_o \qquad \text{(B.4)}$$

where V_o is the volume occupied at standard pressure. Substituting V from equation (B.4) into equation (B.2), the flow velocity becomes

$$v = \frac{V_o}{tA} \frac{P_o}{P} = \frac{H}{A} \frac{P_o}{P} \qquad \text{(B.5)}$$

where $H \equiv \frac{V_o}{t}$. H is the standard flow rate given in SCCM.

As stated in the text, the residence time is defined as the length of time that a portion of the gas stays in the discharge before it is sampled by the spectrometers. The residence time is given by

$$T = \frac{1}{v} \qquad \text{(B.6)}$$

where l is the length from the cathode to the sampling orifice. Substituting the flow velocity from equation (B.5) into equation (B.6), the residence time becomes:

$$T = \frac{AlP}{HP_o} \tag{B.7}$$

When the flow of gas through the discharge tube reaches steady state, the pressure remains constant and the flow in is equal to the flow out. Under this condition of steady state, the total number of molecules in the experimental region of interest (i.e., from the cathode to the sampling orifice) is given by

$$N = n_o HT \tag{B.8}$$

where T is the residence time of the gas, H is the total flow rate, and n_o is the number density of molecules in a standard cubic centimeter. If the flow contains a mixture of gases, then H is just the sum of the individual flow rates of all the gases that constitute the mixture:

$$H = \sum_s H_s \tag{B.9}$$

Substituting the total flow rate from equation (B.9) into equation (B.8), the total number in the experimental region is given by

$$N = n_o T \sum_s H_s \qquad \text{(B.10)}$$

Using equation (B.8), the number density is

$$n = \frac{N}{Al} = n_o \frac{T}{Al} \sum_s H_s$$

$$n = n_o \frac{P}{HP_o} \sum_s H_s$$

$$n = n_o \frac{P}{P_o} \qquad \text{(B.11)}$$

where P is the total pressure of the gas mixture. The total number of a single component is given by $n_o T H_s$, and the number density by $n_o T H_s / Al$ so that the fractional amount of species s is given by

$$\alpha_s = \frac{n_s}{n} = \frac{H_s}{\sum_s H_s}$$

$$\alpha_s = \frac{H_s}{H} \qquad \text{(B.12)}$$

Expression (B.12) uses the fact that the residence times of all the gas components are the same.

Appendix C

Important Reactions and Rate Constants

CO_2/Ar

	Reaction	Rate Constant (300°K)	Reference
1.	$CO_2 + e^- \rightarrow CO + O + e^-$	5.4×10^{-11} cm^3 s^{-1}	*
2.	$O + O + M^{**} \rightarrow O_2 + M$	7.2×10^{-33} cm^6 s^{-1}	6
3.	$O_2 + e^- \rightarrow O + O + e^-$	1×10^{-9} cm^3 s^{-1}	18

CO_2/N_2/Ar

1.	$CO_2 + e^- \rightarrow CO + O + e^-$	1.7×10^{-10} cm^3 s^{-1}	*
2.	$O + O + M \rightarrow O_2 + M$	7.2×10^{-33} cm^6 s^{-1}	6
3.	$O_2 + e^- \rightarrow O + O + e^-$	1×10^{-9} cm^3 s^{s-1}	18
4.	$N_2 + e^- \rightarrow N + N + e^-$	1×10^{-9} cm^3 s^{-1}	***
5.	$N + N + M \rightarrow N_2 + M$	4.4×10^{-33} cm^6 s^{-1}	6
6.	$N + O_2 \rightarrow NO + O$	8.5×10^{-17} cm^3 s^{-1}	6
7.	$N + O + M \rightarrow NO + M$	1×10^{-32} cm^6 s^{-1}	6
8.	$N + NO \rightarrow N_2 + O$	2.7×10^{-11} cm^3 s^{-1}	6
9.	$O + NO_2 \rightarrow O_2 + NO$	9.2×10^{-12} cm^3 s^{-1}	6

CO_2/He/Ar

1.	$CO_2 + e^- \rightarrow CO + O + e^-$	2.2×10^{-10} cm^3 s^{-1}	*
2.	$O + O + M \rightarrow O_2 + M$	7.2×10^{-33} cm^6 s^{-1}	6
3.	$O_2 + e^- \rightarrow O + O + e^-$	1×10^{-9} cm^3 s^{-1}	18

CO_2/N_2/He/Ar

1.	$CO_2 + e^- \rightarrow CO + O + e^-$	2.3×10^{-10} cm^3 s^{-1}	8
2.	$O + O + M \rightarrow O_2 + M$	7.2×10^{-33} cm^6 s^{-1}	6

3.	$O_2 + e^- \rightarrow O + O + e^-$	1×10^{-9} cm^3 s^{-1}	18
4.	$N_2 + e^- \rightarrow N + N + e^-$	1×10^{-9} cm^3 s^{-1}	***
5.	$N + N + M \rightarrow N_2 + M$	4.4×10^{-33} cm^6 s^{-1}	6
6.	$N + O_2 \rightarrow NO + O$	8.5×10^{-17} cm^3 s^{-1}	6
7.	$N + O + M \rightarrow NO + M$	1×10^{-32} cm^6 s^{-1}	6
8.	$N + NO \rightarrow N_2 + O$	2.7×10^{-11} cm^3 s^{-1}	6

*The average rate constant calculated by equation (4.8).

**All Species.

***Assumed rate constant.

Appendix D

Electron Transport Parameters

The electron drift velocities of the experimental mixtures were obtained from the following graphs. These drift velocities allowed an electron number density to be computed. Although the mixtures are not identical to the ones used in the experiment, they represent the best match. Figs. 17, 18, 19, and 20 were used for the following respective experimental mixtures: CO_2/Ar, CO_2/N_2/Ar, CO_2/He/Ar, and CO_2/N_2/He/Ar. Although not used in the thesis, U_k and $\overline{U}$ are the characteristic and average electron energies, respectively.

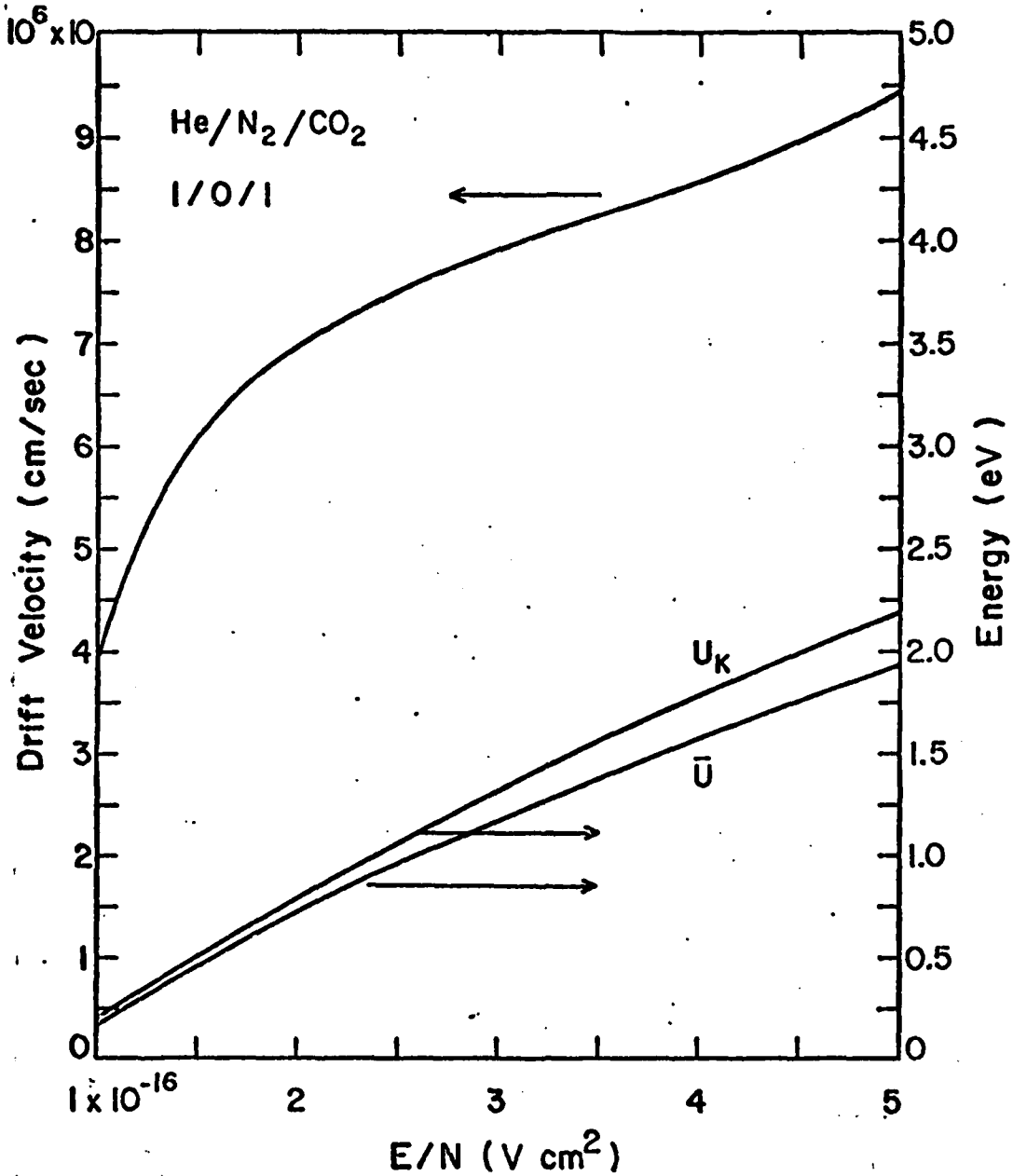

Figure 17. Electron Transport Parameters Used for the 90% CO_2/10% Ar Discharge (Ref 9)

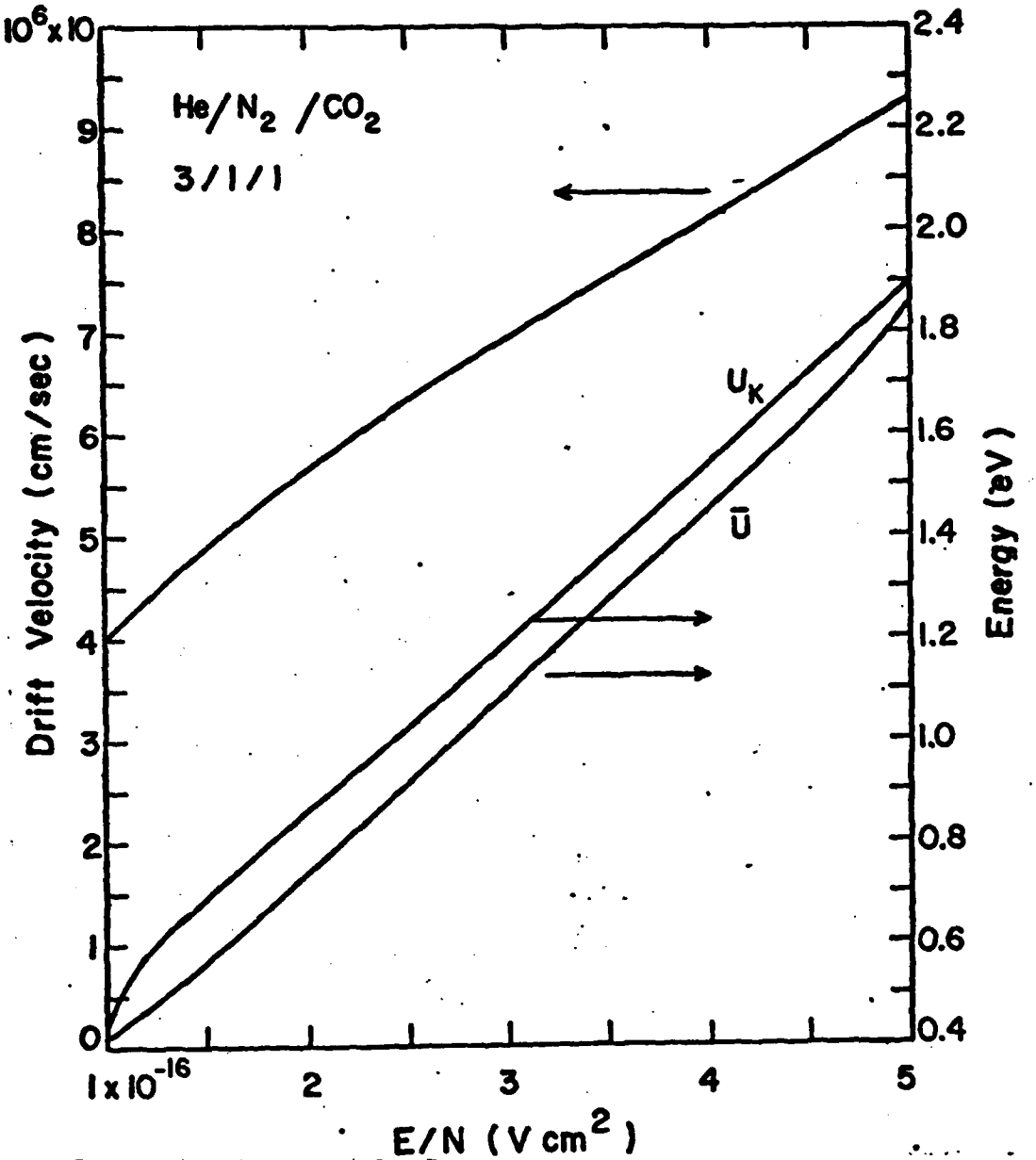

Figure 18. Electron Transport Parameters Used for the 40% CO_2/50% N_2/10% Ar Discharge (Ref 9)

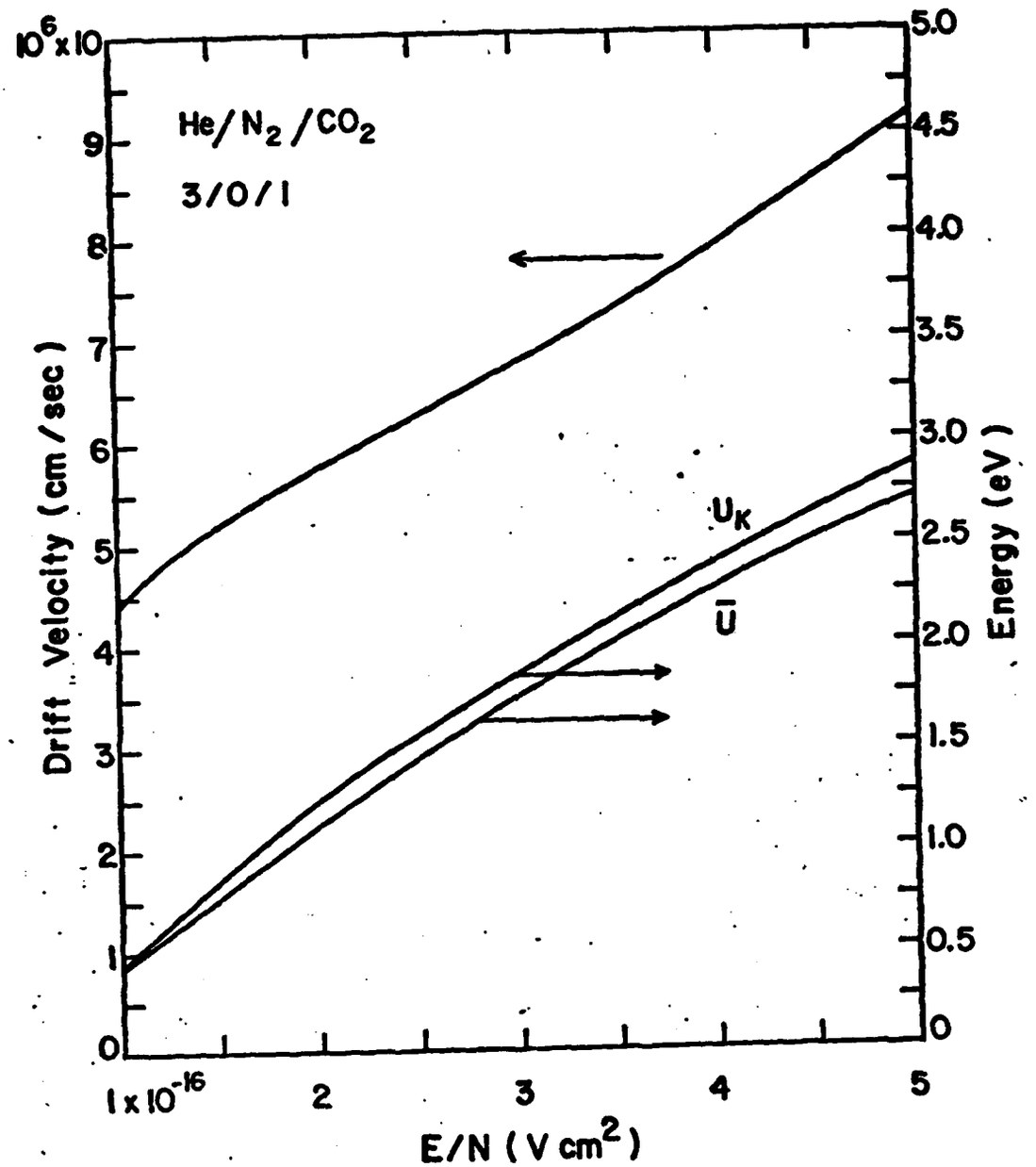

Figure 19. Electron Transport Parameters Used for the 10% CO_2/80% He/10% Ar Discharge (Ref 9)

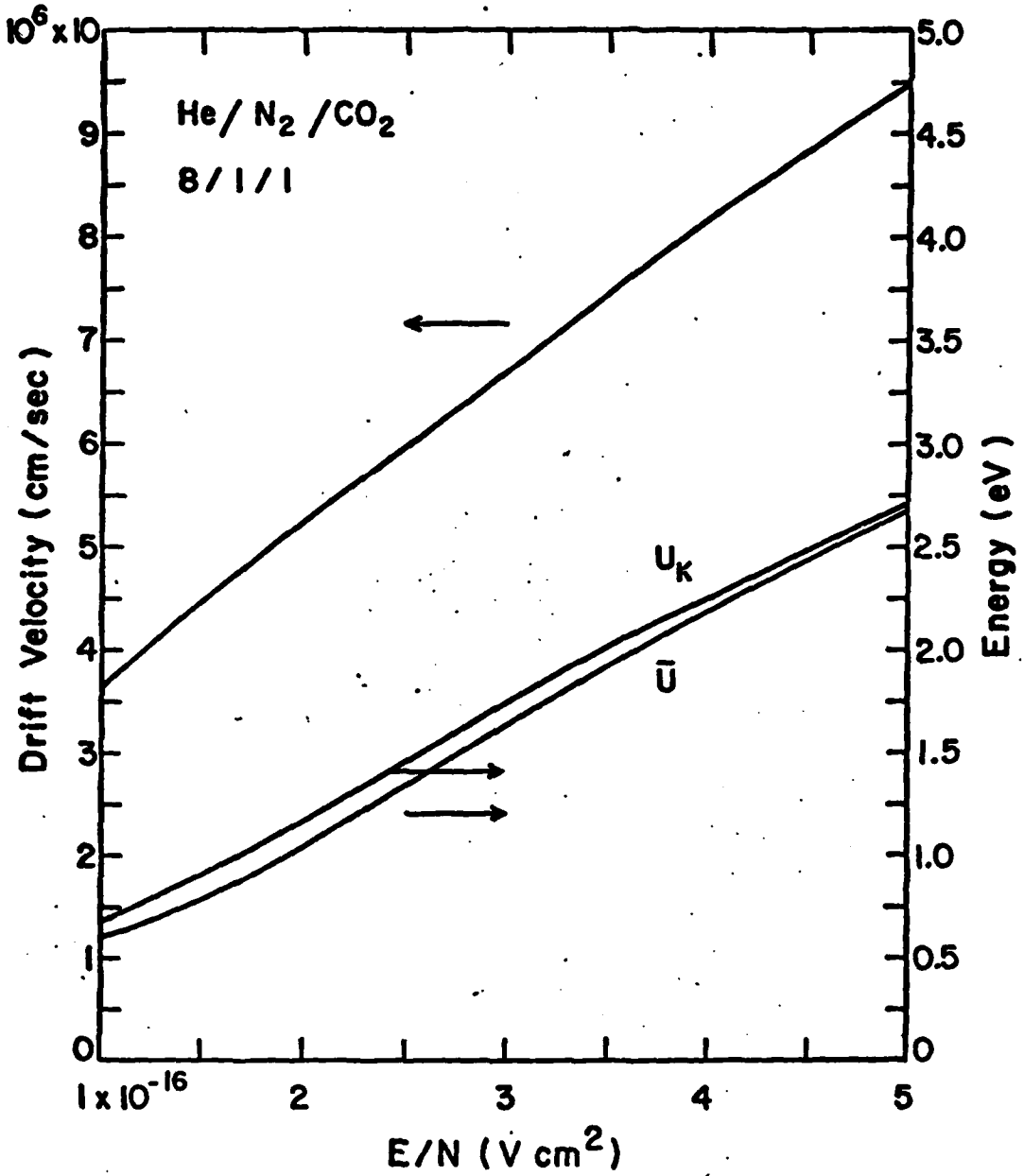

Figure 20. Electron Transport Parameters Used for the 8% CO_2/11% N_2/71% He/10% Ar Discharge (Ref 9)

UNCLASSIFIED

SECURITY CLASSIFICATION OF THIS PAGE (When Data Entered)

REPORT DOCUMENTATION PAGE		READ INSTRUCTIONS BEFORE COMPLETING FORM
1. REPORT NUMBER AFIT/GEP/PH/78D-13	2. GOVT ACCESSION NO.	3. RECIPIENT'S CATALOG NUMBER
4. TITLE (and Subtitle) SYNTHESIS OF THE PLASMA CHEMISTRY OCCURRING IN HIGH POWER CO_2 LASERS		5. TYPE OF REPORT & PERIOD COVERED MS Thesis 6. PERFORMING ORG. REPORT NUMBER
7. AUTHOR(s) David E. Toodle 2nd Lt., USAF		8. CONTRACT OR GRANT NUMBER(s)
9. PERFORMING ORGANIZATION NAME AND ADDRESS Air Force Institute of Technology (AFIT-EN) Wright-Patterson AFB, Ohio 45433		10. PROGRAM ELEMENT, PROJECT, TASK AREA & WORK UNIT NUMBERS 61102F 23015213
11. CONTROLLING OFFICE NAME AND ADDRESS High Power Branch (AFAPL/POD) Air Force Aero Propulsion Laboratory Wright-Patterson AFB, Ohio 45433		12. REPORT DATE December 1978 13. NUMBER OF PAGES 83
14. MONITORING AGENCY NAME & ADDRESS(if different from Controlling Office)		15. SECURITY CLASS. (of this report) UNCLASSIFIED 15a. DECLASSIFICATION/DOWNGRADING SCHEDULE

16. DISTRIBUTION STATEMENT (of this Report)

Approved for public release; distribution unlimited

17. DISTRIBUTION STATEMENT (of the abstract entered in Block 20, if different from Report)

18. SUPPLEMENTARY NOTES

Approved for public release;
IAW AFR 190-17

J. P. HIPPS, MAJOR, USAF 19 Jan 79

19. KEY WORDS (Continue on reverse side if necessary and identify by block number)

CO_2 Lasers
Plasma Chemistry
Electric-Discharge Lasers
Discharge Chemistry
Mass Spectrometry of Plasmas
Glow Discharges

20. ABSTRACT (Continue on reverse side if necessary and identify by block number)

The neutral chemistry of the following mixtures have been studied by using a quadrupole mass spectrometer and a theoretical model: CO_2/Ar, N_2/Ar, CO_2/N_2/Ar, CO_2/He/Ar, and CO_2/N_2/He/Ar. CO_2 dissociation occurs by direct electron impact and appears to depend on initial CO_2 concentration and mixture. Very little N_2 dissociation occurs in a pure N_2 discharge; however, the dissociation

DD FORM 1 JAN 73 1473 EDITION OF 1 NOV 65 IS OBSOLETE

UNCLASSIFIED

SECURITY CLASSIFICATION OF THIS PAGE (When Data Entered)

of N_2 increases when it is added to a mixture containing CO_2. This dissociation is less than 1%. Consequently, the dominant nitrogen oxide in mixtures containing CO_2 and N_2 is NO, and the concentration of NO never exceeds 1%. The species CHO and CH_2O are present at high discharge currents if there is a small amount of water contamination in mixtures containing CO_2.